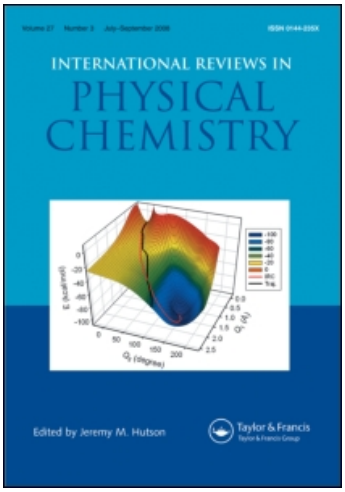

International Reviews in Physical Chemistry
Publication details, including instructions for authors and subscription information:
http://www.informaworld.com/smpp/title~content=t713724383

Recent advances in the visible and UV spectroscopy of metal dication complexes

Hazel Cox[a]; Anthony J. Stace[b]
[a] Department of Chemistry and Biochemistry, University of Sussex, Falmer, Brighton BN1 9QJ, UK [b] Department of Physical Chemistry, School of Chemistry, The University of Nottingham, University Park, Nottingham NG7 2RD, UK

First published on: 08 September 2010

To cite this Article Cox, Hazel and Stace, Anthony J.(2010) 'Recent advances in the visible and UV spectroscopy of metal dication complexes', International Reviews in Physical Chemistry, 29: 4, 555 — 588, First published on: 08 September 2010 (iFirst)
To link to this Article: DOI: 10.1080/0144235X.2010.511774
URL: http://dx.doi.org/10.1080/0144235X.2010.511774

International Reviews in Physical Chemistry
Vol. 29, No. 4, October–December 2010, 555–588

Taylor & Francis
Taylor & Francis Group

Recent advances in the visible and UV spectroscopy of metal dication complexes

Hazel Cox[a]* and Anthony J. Stace[b]*

[a]*Department of Chemistry and Biochemistry, University of Sussex, Falmer, Brighton BN1 9QJ, UK;* [b]*Department of Physical Chemistry, School of Chemistry, The University of Nottingham, University Park, Nottingham NG7 2RD, UK*

(*Received 24 May 2010; final version received 26 July 2010*)

Experimental techniques developed during the past 15 years have demonstrated that it is possible to prepare stable metal dication complexes, such as $[Cu(NH_3)_N]^{2+}$ and $[Ni(H_2O)_N]^{2+}$, in the gas phase. The significance of these complexes lies in the fact that they contain metal ions that are in their more common charge state, and therefore, a link between their properties and those found for the same ions in the condensed phase is readily accessible. In this review, we focus on one aspect of the study of these ion complexes, and that is their visible and ultraviolet (UV) spectroscopy. Current experimental techniques for recording spectra in the gas phase are discussed together with the theoretical methods required to interpret the spectra of metal dication complexes. An attempt is made to identify any barriers that might exist to measuring the optical spectra of metal dication complexes using current ion beam technology, where a typical experiment will involve measuring either photofragment yield or ion beam depletion as a function of laser wavelength. One very obvious area of spectroscopy to be explored, and one that is unique to transition metal complexes, is ligand field spectroscopy. Estimates of photofragment yields based on typical absorption cross sections and the kinetics of fragmentation highlight the difficulties involved in measuring such spectra. Of the theoretical techniques currently available for calculating spectral transitions, the method most commonly used for metal complexes is time-dependent density functional theory (TDDFT). Using selected examples, it is shown that although TDDFT is, for the most part satisfactory, extreme caution should be exercised when investigating the electronic states of open-shell complexes. An obvious conclusion to emerge is that a theoretical method that predicts the correct ground state geometry of an open-shell complex (and is free from spin contamination) does not necessarily yield the correct electronically excited states due to multi-electron character and/or spin contamination in the excited state manifold. It is anticipated that the development of experimental techniques that can record accurate electronic spectra will provide new and more demanding benchmarks for the refinement of theoretical methods.

Keywords: gas phase; metal dications; UV/Vis spectroscopy; TDDFT; excited states

*Corresponding authors. Email: h.cox@sussex.ac.uk; Anthony.Stace@nottingham.ac.uk

ISSN 0144–235X print/ISSN 1366–591X online

DOI: 10.1080/0144235X.2010.511774
http://www.informaworld.com

Contents PAGE

1. Introduction

One of the prime objectives of cluster science is to seek evidence of how properties exhibited by small isolated collections of atoms and molecules evolve into those displayed by the corresponding bulk materials. For example, the ionisation energy of a single atom becomes the work function of a piece of metal. In some cases, this evolution spans many hundreds, sometimes even thousands of atoms or molecules; however, there is one property where more modest numbers of species are involved, and that is ion solvation. Very significant progress has been made over the past three or four decades on the study of the thermodynamic properties of singly charged cations, anions and metal ions in the presence of small numbers of solvent molecules [1,2]. From these experiments and the accompanying theory it is possible to demonstrate that the essential thermodynamics of ion solvation can be understood through the association of an ion, such as Na^+, with approximately six water molecules. What ultimately limits the applicability of these experiments is the range of systems that are both singly charged and have relevance to the condensed phase. Many experiments have been performed on, for example, the gas phase chemistry and spectroscopy of Ni^+ complexes with solvent molecules, but this ion is not known to exist in the condensed phase. However, the value of this work should not be underestimated. Experimental results on singly charged complexes still present demanding tests for theory and provide a vital source of high-accuracy binding energy data to validate computational methodologies. The data also allow systematic trends in chemistry and ligand coordination to be evaluated in terms of ionic radii, differing electron spin configurations and the development of hydrogen bonded networks.

The past few years has seen a significant increase in the number of new experiments that have been developed to generate and study multiply charged metal–ligand complexes in the gas phase [3]. These experiments have demonstrated that it is possible to prepare a wide range of complexes containing first-row transition metals in charge states commonly observed in condensed phase chemistry [4], i.e. Cr(II) [5], Mn(II) [6], Co(II) [7],

Fe(II) [8], Ni(II) [9] and Cu(II) [10–12]. Frequently, these experiments are undertaken in association with ligands that occupy pivotal positions in traditional transition metal chemistry [4], e.g. H_2O, NH_3, pyridine and bipyridine. Prime examples of the type of complex that can be prepared include $[Cu(H_2O)_N]^{2+}$ [10], $[Cu(NH_3)_N]^{2+}$ [11] and $[Ni(H_2O)_N]^{2+}$ [9]. Although successful, the experimental problems that need to be overcome to generate these ions should not be underestimated. In order to understand what is involved, we can begin by deconstructing a common procedure, dissolving copper sulphate in water, into single collision steps between the constituent cation and a water molecule (the fate of SO_4^{2-} is not considered, but this dianion has been the subject of several recent studies in the gas phase [13,14]). Figure 1 shows the potential energy differences associated with interactions between Cu^+/Cu^{2+} and a water molecule. The preparation of a complex of the form Cu^+H_2O from the separate species is comparatively straightforward: the ionisation energy of a water molecule is higher than that of a copper atom and so following a collision, the charge is naturally located on the metal. This route has been used with considerable success to prepare gas phase complexes from singly charged metal ions and molecules [1,2]. However, the same is not true of Cu^{2+}; based on the energy differences shown, a collision between Cu^{2+} and H_2O should lead immediately to Cu^+ and H_2O^+ (or possibly $CuOH^+ + H^+$) and the release of a considerable amount of kinetic (thermal) energy. Clearly, this does not happen when copper sulphate is dissolved in water; otherwise the process would be extremely hazardous! By being associated with many water molecules, Cu^{2+} is stabilised in solution with both charges remaining on the metal. However, what this means for the preparation of complexes in the gas phase is that the traditional (and very successful) single collision approach does not work [1,2]. Therefore, techniques have to be found (pick-up [3,15] and electrospray [8,16]) that can generate metal dications and trications that are already encapsulated in a stable solvent environment when they enter the gas phase.

The ability to generate such ionic complexes with sufficient signal strength for quantitative study (10^7 ions s^{-1} $\sim 10^{-12}$ A) offers an opportunity to perform spectroscopic measurements. Again, ease of formation means that many experiments of this nature have concentrated on singly charged ions [17] where most recently, the recording of UV/visible

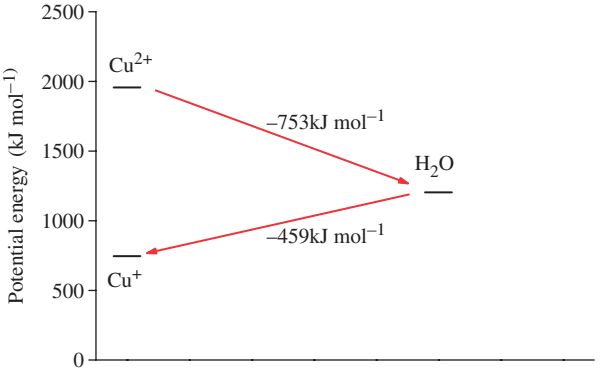

Figure 1. [Colour online] Schematic representation of the potential energy differences between $Cu^{+/2+}$ and a single water molecule.

spectra has given way to measurements at infrared (IR) wavelengths [18,19]. Compared with electronic excitation, the latter approach appears to be far more sensitive to the development of solvent shell structure, particularly when used in conjunction with rare gas tagging. The addition of a weakly bound argon atom to a complex takes photodissociation from being a multiphoton IR process to one that requires just a single photon [20].

Similar progress has been made in the development of techniques and methodologies for modelling the behaviour of metal cation-molecule complexes in both the gas phase and the condensed phase. In fact, such condensed phase calculations are often performed on isolated 'gas phase' structures, which may then be embedded in a solvent approximated using a dielectric continuum model, such as conductor-like screening model (COSMO) [21] or polarized continuum model (PCM) [22]. The inclusion of solvent effects can be extremely important in accurately modelling solvachromatic shifts of, e.g. metal-to-ligand charge transfer (MLCT) transitions in the condensed phase [23], and/or combining the quantum-mechanical calculations with molecular dynamics (MD) to model and explain the dynamic effects of both intramolecular and environmental fluctuations on spectra and excited-state behaviour.

As noted in a recent review on the gas phase chemistry of coinage metals [24], it is important to acknowledge that the huge progress in understanding the chemistry of metal-containing systems *via* combined theoretical and experiment studies, could not have been achieved without the rapid progress in density functional theory (DFT) that has been made in the last two decades [25]. This is because DFT includes electron correlation in the calculations at a computational cost considerably less than that of post-Hatree–Fock methodologies yet with a similar accuracy. Thus DFT is often the method of choice, if not the only viable option, for medium to large metal-containing species. For an excellent review of DFT and its recent progress in applications to transitional metal chemistry, see [26]. As DFT has flourished, so many new functionals have appeared, described aptly by Perdew's Jacob's ladder [27,28] for the five generations of DFT functionals from Hartree World to Chemical Heaven. There has also necessarily been a large number of benchmarking studies each comparing the performance of several well-established density functionals with the most recent alternatives. For a good review on the general performance of density functionals, including a brief historical background and a summary of benchmarking studies performed from 2003 to 2007 see [29] and references therein. New functionals continue to appear with improved performance and it is likely that the selection of a particular functional will continue to depend both on the property and type of system under study and on the computational resources available.

State-of-the-art quantum chemistry of the excited state has been reviewed [30] along with a review of single-reference *ab initio* methods for calculating the excited states of large molecules [31]. From these detailed overviews of commonly employed quantum-chemical methods and strategies it is clear that, in order to have an overall accurate and balanced description of all types of excited state (closed- and open-shell) in all types of molecular system, the only widely applicable methods are the multi-reference (MR) perturbative methods, such as complete active space perturbation theory of second order (CASPT2). However, even this approach is not completely problem-free due to the selection and size of the reference wavefunction [30]. It is acknowledged [30] that time-dependent density functional theory (TDDFT), which evaluates vertical electronic excitation energies using Kohn–Sham (KS) response theory (by considering the linear response of the electron

density to a time-dependent field in the adiabatic approximation, the excitation energies may be determined as the poles of the frequency-dependent polarizability), has no *ab initio* rival when computing excited states in large molecules, and these authors predict that more excited state calculations will be carried out in the near future using TDDFT. Indeed this has started to happen and as indicated below, TDDFT is beginning to enjoy the attention that DFT has received in the last decade.

There is one aspect of condensed phase spectroscopy that is unique to transition metals, and in particular metal cations, and that is ligand field (LF) spectroscopy, where UV/visible radiation is used to promote electronic transitions between d-electron energy levels centred on metal cations [32]. Thus, the prospect of being able to generate Ni(II) and Cu(II) complexes in the gas phase offers a unique opportunity to study the progression of LF electronic transitions as a function of the number and type of ligand. In view of the almost complete absence of any structure associated with most condensed phase LF spectra [32], any advance that might offer evidence of either spin–orbit coupling or vibrational structure would appear worth pursuing.

The purpose of this article is to outline the current status regarding the gas phase spectroscopy of metal dication complexes, both in terms of the types of experiment that can be undertaken and how well theory performs at being able to account for the results. Also discussed is how theory might progress computationally in order to take into consideration such factors as spin–orbit coupling in the excited states of open- and closed-shell metal–ligand complexes. Examples are provided of where experiment and theory (TDDFT) have complemented each other and also examples were limitations in the computational methodology have prevented quantitative assignment of the experiment; thus providing perspectives for future research as well as methodological developments.

One very obvious problem that applies equally to gas phase experiments on transition metal cations as it does to condensed phase spectral measurements is that LF or *d–d* electronic transitions are forbidden [32]. Electronic transitions between states of the same parity are Laporte forbidden, which means that in the absence of contributing factors, such as intensity stealing or vibronic coupling [32], absorption cross-sections will be far lower than those typically seen in other areas of gas phase ion spectroscopy (see below). Having said that, there have already been several important contributions by Posey *et al*. [33] and Metz *et al*. [9,34,35] to the development of new experiments for the study of transition metal ion spectroscopy in the gas phase. In addition, our work has combined experiment and theory in order to understand the origins of electronic transitions observed in gas phase Cu(II) and Ag(II) complexes at visible wavelengths [36,37]. However, none of these earlier studies have managed to realise an important experimental objective, which is that of obtaining high-resolution spectra and, in several cases, charge transfer rather than LF transitions have been observed. As will be shown below, more recent developments in experimental technique have meant that for Zn(II) complexes it has been possible to resolve individual electronic transitions.

2. Experimental

A typical experiment will consist of two components: a method of preparing the cations and a method for recording their spectra. Preparation can take the form of either

electrospray [9,15,16,33,34] or the pick-up technique [36,37] and both have been used successfully to record spectra. Ion preparation and photoexcitation can take place in several different types of mass spectrometer, including high-voltage sector machines, quadrupole mass spectrometers and ions traps. Each has advantages (and disadvantages) and some of those may become apparent from the material discussed here. The discussion here will concentrate on two instruments: a sector machine (Vacuum Generators ZAB-E reverse geometry mass spectrometer) and a hybrid quadrupole-ion trap instrument that originates from a Finnegan ITMS system. Signal intensities, detection efficiencies, timescales, etc., will be identified for each particular instrument. Reference will also be made to situations where significant differences in performance exist between the two instruments.

Figure 2 shows a schematic diagram of an apparatus that has been used with considerable success in our laboratory to study a wide range of metal–ligand complexes, and is currently used to record LF spectra. Argon carrier gas at a pressure of 30–50 psi is seeded with the desired solvent, which then undergoes adiabatic expansion through a pulsed, 200 μm diameter conical nozzle, leading to the formation of neutral mixed argon–solvent clusters. Most of the solvents (ligands) used are in the liquid state, and are held in a stainless steel reservoir through which the carrier gas passes. Collimation of the beam takes place downstream from the nozzle with a 1 mm diameter skimmer before passing into the pick-up region. In this next section of the apparatus, metal pieces are held in a pyrolytic boron nitride or aluminium oxide crucible which can be heated in an effusion cell (DCA Instruments, Model EC-40-63-21) to temperatures in excess of 1500°C. These conditions have been found sufficient to vaporise a significant number of metals to a partial pressure of approximately 10^{-2} mbar. A further range of ovens using carbon filaments can access temperatures up to 2000°C, which means that there are only five metals in the periodic table that cannot be studied in this way.

The metal vapour flows into the path of the molecular beam where the mixed argon–solvent clusters 'pick-up' a metal atom (M) to produce neutral clusters of varying composition, including $M(L)_N(Ar)_M$, $M(L)_N$ and $M(Ar)_M$. If the temperature of the oven is too high, the molecular beam intensity is diminished due to scattering by metal atoms. A shutter positioned at the exit to the oven is used to confirm the presence of metal within a particular ion that has been chosen for further study. On entering the ion source of a reverse geometry Vacuum Generators ZAB-E mass spectrometer, the clusters are ionised using high-energy electron impact (70–100 eV). This procedure generates a wide range of singly, doubly and triply charged cluster ions, some of which contain a metal ion.

Charged clusters are then accelerated at 5 kV through the first field-free region (FFR) into the magnetic sector of the mass spectrometer where they are selected according to their mass to charge ratio. These ions then enter a long FFR (~1.5 m) of the mass spectrometer where they can be irradiated with the output of two separate laser systems. In some of the earlier experiments an optical parametric oscillator (OPO) laser (Spectra-Physics MOPO-710) pumped with an injection-seeded Nd:YAG laser (Spectra-Physics GCR-200) has been used to cover the wavelength of ranges 440–690 nm (signal) and 730–1200 nm (idler). In contrast, more recent studies have concentrated on the UV region of the spectrum, and for these experiments laser radiation with a tuning range of 220–310 nm has been generated by frequency-doubling the output from a dye laser (SIRAH – PrecisionScan) pumped with a Nd:YAG laser (Surelite III) operating at 355 nm.

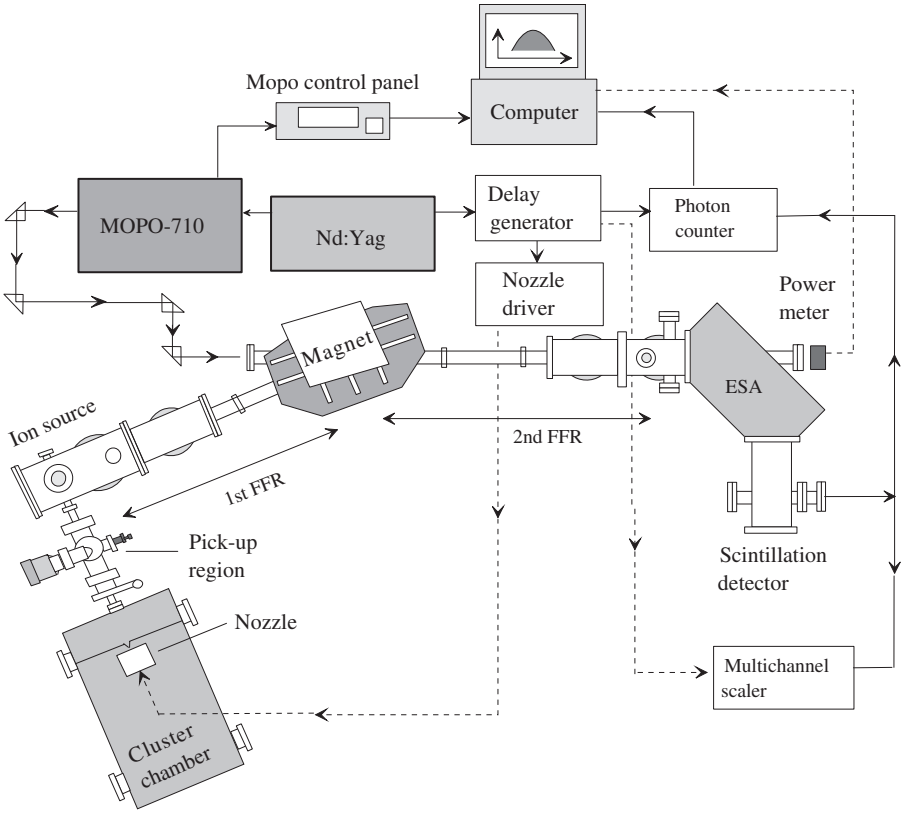

Figure 2. Schematic diagram of an apparatus that has been used to record gas phase LF spectra from complexes containing Cu(II) and Ag(II). Details of the experiment are presented in the main text. Reprinted with permission from [43]. Copyright 2007, American Institute of Physics.

Data points at a single wavelength often represented an average of 3000–4000 laser shots, and many of the published spectra (see below) have taken up to 24 h of continuous measurement to record [36,37]. Both the pick-up system and the mass spectrometers are able to maintain stability over this period of time and, typically, an oven can operate effectively for 48 h before needing to be replenished.

Following irradiation, the m/z values of any ionic fragments are identified by passing the ion beam through an electrostatic analyser (ESA). This particular linked-scanning technique, which decouples the magnetic and electric sectors, is normally referred to as a Mass-analysed Ion Kinetic Energy (MIKE) scan [38]. Scanning the ESA provides an almost unambiguous method for distinguishing between fragment ions originating from the loss of neutral ligands and the products of charge transfer. When doubly charged species are produced in the ion source, they acquire twice the kinetic energy of mass coincident singly charged ions. Accordingly, when charge transfer occurs to produce two singly charged daughter ions, these are transmitted at kinetic energies double that of a mass coincident singly charged species formed in the ion source. With the ion source

operating at 5 kV, it is necessary to scan the ESA such that ions with kinetic energies between 0 and 10 keV are transmitted through to the detector in order to identify all possible charge transfer products. Singly charged ions created by charge transfer are frequently accompanied by an extensive release of kinetic energy, which appears as a consequence of repulsion between the two separating positively charged daughter ions (Coulomb explosion). Thus, peaks associated with charge transfer processes are often much broader than neutral loss peaks, which makes identification easier, but accurate mass assignment more difficult. Ion detection is *via* a Daly scintillation detector linked to a lock-in amplifier (Stanford Research Systems SR850), which gives phase-sensitive detection referenced with respect to the train of nozzle pulses. For very weak signals, the scintillation detector can be linked to a photon counting tube, the output of which is fed to a gated photon counter (Stanford Research Systems SR400).

In the experiments undertaken by Metz *et al*. [9,34] and more recently within the authors own laboratory [39], an ion trap has been used in an attempt to increase the number of ions available for photoexcitation. In these experiments, mass-selected ions are fed into an ion trap that serves as an integrating device and accumulates ions for periods of up to 1 s. The ions are then irradiated and finally expelled from the trap to give a photofragment mass spectrum. In addition to operating with increased ion number densities, the ion trap offers further advantages over the use of sector or quadrupole instruments. By ramping the RF trapping signal to expel the contents, the intensities of all the ion fragments can be monitored simultaneously, and by retaining photoexcited ions for up to 1 s it is possible to shift the timescale over which photo-induced and/or unimolecular decay is observed by four orders of magnitude. An example of the consequences of this latter operation is given later. Details of the design of an ion trap apparatus built by Wu *et al*. together with estimates of signal strength and performance parameters can be found in reference [39].

As an extension to experiments on trapped ions, the introduction of a mechanism for cooling the ions can lead to significant improvements in how well individual electronic states can be resolved. Although there has been remarkable progress in the use of closed cycle cooling systems in the study of cold molecular ions, where temperatures as low as 10 K have been achieved [40], experiments to date on metal dication complexes have used liquid nitrogen cooling, which can bring the internal temperature of ions down to approximately 100–150 K. Even this modest reduction in temperature can help resolve discrete transitions between electronic states.

3. Signal strengths and the kinetics of photofragmentation

The recording of optical spectra follows a common pattern – ions of a particular m/z ratio are selected and photoexcited with tuneable laser radiation. The absorption of a photon on the part of a complex leads to dissociation and the resultant photofragmentation signal is monitored as a function of laser wavelength to provide a spectrum. The degree of photofragmentation can be followed in two ways: either the ionic products can be identified and monitored or the depletion of parent ion signal can be recorded. The former has the advantage of sensitivity in that an ion signal can be recorded against zero background, but the signals can also be very weak. Knowledge of the photofragmentation pathway can also be helpful in the identification of electronic transitions that have

a significant charge transfer component [37]. Depletion measurements have the advantage that they reflect the sum of all photofragmentation channels, but the disadvantage that spectra are derived from the difference of two large numbers. Again, both approaches have been used successfully [37]. Figure 3 shows two examples of photofragment signals recorded following the excitation of $[Cu(pyridine)_4]^{2+}$ at 266 nm. There are two reaction channels:

$$[Cu(pyridine)4]^{2+} + h\nu \rightarrow [Cu(pyridine)_3]^{2+} + \text{pyridine} \quad (1)$$

$$\rightarrow Cu^{+}(pyridine)_2 + pyridine^{+} + pyridine \quad (2)$$

The ion signals shown in Figure 3 were recorded by stepping the ESA and counting ions on a multichannel scalar (Stanford Research SR450). As can be seen, the laboratory-frame kinetic energy release profile for pathway (1) is quite narrow and probably reflects the bandwidth of the ESA with the energy resolving slits set to their maximum values. The width and shape are characteristic of a statistical partitioning of internal energy

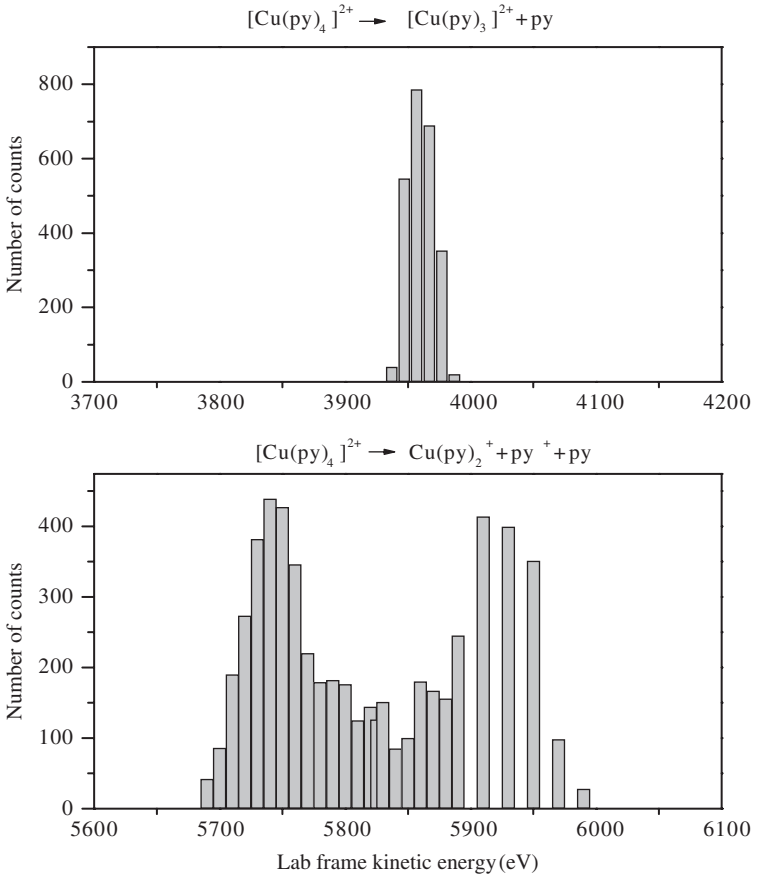

Figure 3. Laboratory-frame kinetic energy profiles recorded following the photoexcitation of $[Cu(pyridine)_4]^{2+}$ at 266 nm. Two photofragmentation pathways are observed: loss of neutral pyridine (upper figure) and charge transfer (lower figure).

following the unimolecular decay of an excited ion. In contrast, the profile recorded for the charge transfer process, pathway (2), is very broad and characteristic of Coulomb explosion, where repulsion between the separating charges has generated substantial centre-of-mass kinetic energy. Maximum signal intensity is derived from fragment ions that have experienced either forward or backward scattering with respect to the flight direction of the ion beam. Similar kinetic energy profiles have been recorded by Faherty *et al.* [41] following the photofragmentation of Co^{2+}/water complexes. As might be anticipated, the collection efficiency of photofragment ions from charge transfer processes, such as (2) above is poor in comparison to pathway (1), where all the fragments are concentrated over a narrow kinetic energy range. Figure 4 illustrates the second of the signal recovery options identified above. In this case, the mass spectrometer has been setup to transmit $[Ag(pyridine)_4]^{2+}$ and the ion signal has been accumulated on a multichannel scalar at the same time as radiation from a laser operating at 266 nm has intersected with the ion beam. As can be seen, photofragmentation has 'burnt' a 25 μs hole in the ion signal, and using gated subtraction an absorption profile can be recorded by monitoring such data as a function of wavelength. Under circumstances, such as those described above where there are two or more competing photofragmentation pathways, the most effective method of measuring an absorption spectrum is by recording signal depletion. The quadrupole ion trap offers an equivalent level of sensitivity in that it can be operated in a mode whereby all of the ions (precursor and fragments) can be monitored simultaneously.

3.1. *Absorption cross-section*

A significant problem facing all experiments of this nature is signal intensity. There are many excellent examples of ion spectroscopy at almost all wavelengths ranging from the

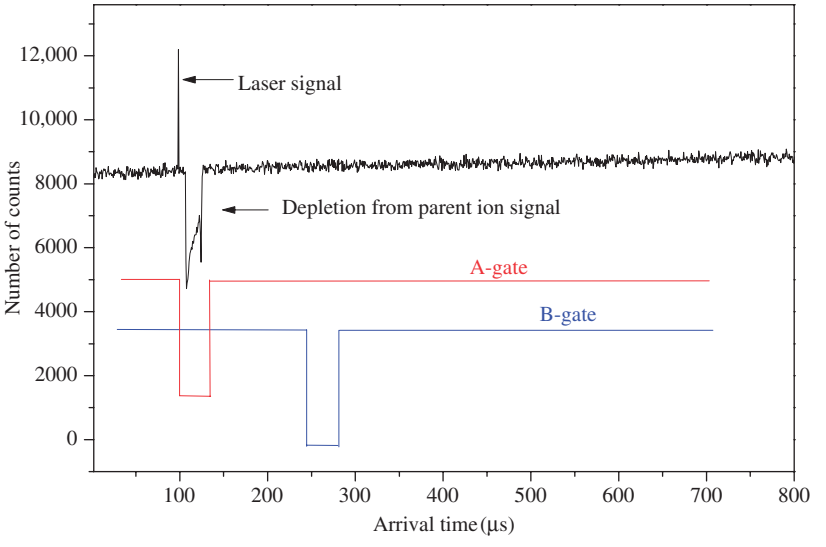

Figure 4. [Colour online] Depletion of the $[Ag(pyridine)_4]^{2+}$ parent ion signal following photoexcitation at 266 nm. The two gates correspond to time windows in a photon counter during which signal is collected. Depletion is recorded as a difference between the two gated signals. Reprinted with permission from [43]. Copyright 2007, American Institute of Physics.

microwave through to the UV [42]. However, most of these experiments have been undertaken either on molecular ions that are generated directly by electron ionisation, in which case the signal strengths are in the region of 10^{-6} A ($\sim 10^{13}$ ion s^{-1}), or on ions that have allowed optical transitions and where the absorption cross sections can be very large. For the least favourable of the processes we would like to study, LF spectroscopy in the gas phase, neither of these factors will apply: the ion flux can be as low as 10^{7} ions s^{-1} (equivalent to an ion current of $\sim 10^{-12}$ A) and the absorption cross section can be at least four orders of magnitude lower than might be expect of, for example, a charge transfer excitation in a transition metal complex [32]. To illustrate the scale of the problem, we can estimate a photofragmention ion yield, N_p, based on the assumption that the number of ion fragments, N_p, is equal to the number of photons absorbed:

$$N_p = N_0[1 - \exp\{\sigma(\nu)\phi\}]$$

where N_0 is the initial ion flux, $\sigma(\nu)$ is the absorption cross section, which for a *d–d* transition is of the order of 50 M^{-1} cm^{-1} ($\sim 10^{-24}$ m^2) [32], ϕ is the photon flux, which for our laser system (Spectra Physics MOPO) is $\sim 10^{21}$ photons $pulse^{-1}$ m^{-2} at ~600 nm. These values give $N_p/N_0 \approx 10^{-3}$. In experiments in the ZAB-E mass spectrometer, a pulsed nozzle is used with a pulse duration of 5 ms, of which the laser 'sees' a window lasting 25 μs (Figure 4) that corresponds to those ions (~50,000) residing in the flight tube at the time the laser is fired. Thus, $N_p \approx 50$ ions per laser pulse. This number would provide an approximate measure of any depletion signal that is recorded under the conditions specified above. If product ion selection/identification is made then there is a second stage of analysis. Fragment ions can emerge from the dissociation process with a spread in their laboratory-frame kinetic energy of ~200 eV if charge transfer/Coulomb explosion is part of the fragmentation process (Figure 3). Fragment analysis on our machine takes the form of an electrostatic kinetic energy analyzer that has an energy band pass of 20 eV with the slits at their maximum wide. Thus, when coupled with fragment ion identification, the ion yield can be fewer than *5 ions per laser shot*. In practice, we can also expect the number of absorptions to be $\gg$ number of photofragments collected, on the grounds that some ions might fluoresce and some fragments might be lost through instrumental discrimination. Despite these problems, techniques exist for single ion counting and spectra have been recorded under the conditions outlined in this section [37,43].

3.2. *Kinetics of photofragmentation*

The above calculations serve to illustrate the scale of the problem with regard to obtaining sufficient signal to record spectra that have quantitative significance. A second problem concerns the conditions under which the measurements are performed. Electron impact ionisation is a very destructive process and one which leaves ions with extensive levels of vibrational and possibly electronic excitation, as confirmed by the frequent observation of unimolecular (metastable) decay. The question then is whether or not the internal energy (temperature) of the ions can be quenched in order to achieve greater spectral resolution. Figure 5 summarises the situation regarding the preparation of ions in a typical mass spectrometer based on an experiment where electron impact ionisation is used. Ions will be formed with a distribution of internal energies (here represented by $f(E)$), with an upper energy limit determined (in an approximate fashion) by the lifetime of an ion with respect

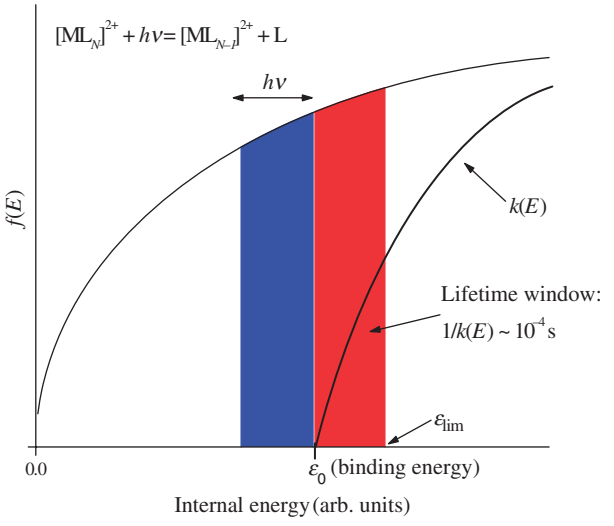

Figure 5. [Colour online] Model of the conditions that could prevail within a photodissociation experiment on $[ML_N]^{2+}$ ions, $f(E)$ represents a distribution of internal energy resulting from electron ionisation, $k(E)$ is the unimolecular rate constant from the loss of a neutral ligand from an ion with energy $\geq \varepsilon_0$ the binding energy (dissociation limit). Below ε_0 the ions could photodissociate because the addition of $h\nu$ would take them above the dissociation limit. Ions with an energy $> \varepsilon_0$ can reach the dissociation region if their lifetime is $> \sim 10^{-4}$ s. To be recorded as such, all photoexcited ions have to fragment within their flight time through the apparatus.

to breaking the weakest metal–ligand bond. Broadly speaking, the distribution can be divided into two components: (i) those ions with an internal energy less than ε_0, the lowest dissociation energy; (ii) those ions with an energy $\geq \varepsilon_0$. The fate of the latter group depends, to some extent, on the type of experiment being undertaken. We shall address the problem from the view point of conditions that prevail in both of the experiments discussed here, noting that the timescale over which ions are held in an experiment will have an influence on subsequent events. In a typical double focusing experiment (either a sector or quadrupole instrument), ions can take up to 10^{-4} s to pass through the apparatus. Thus, ions for which $1/k(E) > 10^{-4}$ s, where $k(E)$ is the rate constant for unimolecular decay at an internal energy E, will maintain an energy $\geq \varepsilon_0$ during their passage through the apparatus and will, on average, survive to reach the detector. These circumstances are summarised in Figure 5, where the region around ε_0 has been highlighted, and from where it is possible to identify the two separate areas that become significant during a photoexcitation experiment: (i) those ions with an internal energy $< \varepsilon_0$ for which the addition of a photon will raise E to a value whereby fragmentation could occur during the remainder of their time in the apparatus; (ii) a less obvious group of ions for which $E \geq \varepsilon_0$, but with a lifetime $> \sim 10^{-4}$ s. The addition of a photon shortens this value such that fragmentation could also occur during the remainder of their time in the apparatus. Obviously, any contribution from the latter group of ions will be strongly influenced by the type of experiment being undertaken. For example, ion trapping could extend the lifetime criterion to ~ 1 s, with the result that the ions being sampled are probably colder.

The exact contribution each of the two regions identified in Figure 5 makes to the total photofragment yield ($m'_{h\upsilon} + m''_{h\upsilon}$) can be summarised in the following equations:

$$E < \varepsilon_0$$

$$m'_{h\upsilon} = \alpha \int_{\varepsilon_0}^{\varepsilon_0 + h\upsilon} f(E - h\upsilon)[1 - \exp\{-k_{h\upsilon}(E)t_4\}]\mathrm{d}E \tag{3}$$

$$E \geq \varepsilon_0$$

$$m''_{h\upsilon} = \alpha \int_{\varepsilon_0}^{\varepsilon_{\lim}} f(E)[1 - \exp\{-k_{h\upsilon}(E + h\upsilon)t_4\}]\mathrm{d}E \tag{4}$$

where $\varepsilon_{\lim}$ satisfies the condition:

$$\exp\{-k(\varepsilon_{\lim})t_3\} \approx 0$$

where t_3 is the time taken by an ion to reach the photoexcitation region, t_4 is the time taken to pass through this region, $f(E)$ is the distribution of internal energy present in a particular series of ions and α is a normalisation constant. These two integrals can be solved numerically with $k(E)$ calculated using Rice–Ramsperger–Kassel–Marcus (RRKM) theory [44] and combined with a functional form for $f(E)$ that has been used in the past to calculate fragment intensities from the decay of cluster ions [45].

To illustrate the importance of the various contributions identified in Equations (3) and (4), calculations have been performed on the system $[\mathrm{Cu(pyridine)}_N]^{2+}$ for $N = 3$–5, which has already been the subject of a recent experimental and theoretical study [37]. The experimental work entailed recording LF spectra in the range 10,000–20,000 cm^{-1}, and DFT was used to predict stable structures, their ligand binding energies, and identify any electronic transitions (using DFT–ΔSCF) that fell within the above wavelength range. Examples taken from the experimental measurements are given below, where in each case spectra were recorded by monitoring the degree of photofragmentation as a function of laser wavelength [37]. The dissociation channel relevant to these calculations is:

$$[\mathrm{Cu(pyridine)}_N]^{2+} + h\upsilon \rightarrow [\mathrm{Cu(pyridine)}_{N-1}]^{2+} + \mathrm{pyridine} \tag{5}$$

To illustrate how effective photons of a particular energy might be at promoting reaction (5), Figure 6 shows the calculated average total binding energy of $[\mathrm{Cu(pyridine)}_N]^{2+}$ complexes plotted as a function of N [46]. At selected data points an arrow has been added that is equivalent in length to the average energy of a visible photon (~200 kJ mol^{-1}). As can be seen, the binding energy increases steeply as a function of size until $N = 4$, at which point it begins to level off. In structural terms, $[\mathrm{Cu(pyridine)}_4]^{2+}$ corresponds to the formation of a stable square-planar confirmation [37], typical of many condensed phase Cu(II) complexes [32]. The calculations show that additional ligands ($N = 5$ and 6) are destabilised through Jahn–Teller distortion [37], which is reflected in the magnitudes of their binding energies. As a consequence, the arrows show that for $N = 5$ and 6, photons at visible wavelengths should be capable of promoting reaction (5), even when the ions contain little or no residual internal energy. However, at $N = 4$ it is clear that dissociation should not occur unless the ions are 'hot' and at $N = 3$ we might predict a mixture of events combining both 'hot' and 'cold' ions.

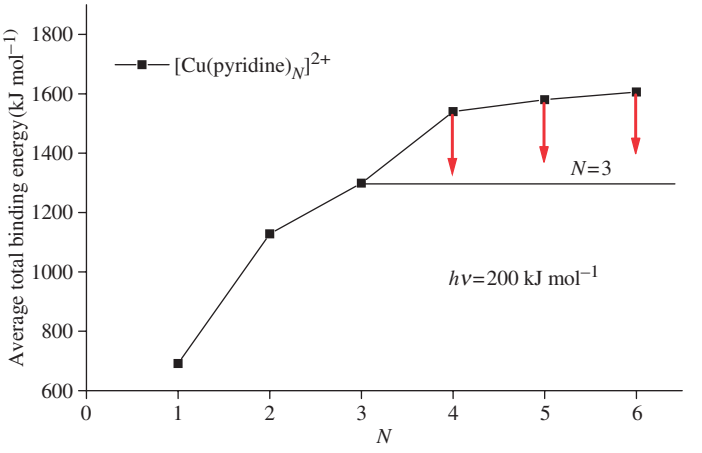

Figure 6. [Colour online] Calculated total binding energy of [Cu(pyridine)$_N$]$^{2+}$ complexes plotted as a function of N. Adapted from [37]. Incremental binding energies are given by the difference between two adjacent values. The length of an arrow reflects the photon energy they represent, which in this case is 200 kJ mol^{-1} (16,700 cm^{-1}).

Figures 7–9 show calculated photofragment yields plotted as a function of wavelength for $N=3$–5, together with experimental results obtained for $N=4$ and 5. No similar experimental data could be recorded at $N=3$. The calculations do not include any information on how the absorption cross-section might vary as a function of wavelength; it is assumed that all ions absorb at every wavelength and that absorption is accompanied by photofragmentation if such a process is energetically favourable. The two individual contributions to the total fragment ion yield identified earlier, have been calculated and are presented separately in Figures 7–9. Figure 7 shows that, depending on the wavelength, any spectrum recorded for [Cu(pyridine)$_3$]$^{2+}$ (or any ion of comparable complexity and binding energy) could be expected to include contributions from both sources. For ions with an internal energy above ε_0, their contribution increases rapidly as a function of E until it reaches a fixed value whereupon every ion in that part of the distribution dissociates. Any further increase in yield then has to come from ions with energies below ε_0, but this does not begin to happen to any significant degree until the photon energy reaches ε_0. To illustrate how the wavelength dependence of the photofragment yield (as opposed to the absorption cross-section) might influence a spectrum, the experimental data from [Cu(pyridine)$_4$]$^{2+}$ has also been included. Figure 8 shows the results of similar calculations on [Cu(pyridine)$_4$]$^{2+}$. As anticipated from the data in Figures 5 and 6, the entire contribution to the photofragment yield comes from ions which already have an energy greater than ε_0. At visible wavelengths, there is no contribution from 'cold' ions. In contrast, the data in Figure 9 shows that for [Cu(pyridine)$_5$]$^{2+}$, a significant fraction of the total ion yield results from 'cold' ions, and that there is now a small, but fixed, contribution from those ions where $E \geq \varepsilon_0$. The latter correspond to ions that live long enough to reach to photoexcitation region, but their residual internal energy is much smaller than that deposited by the photon.

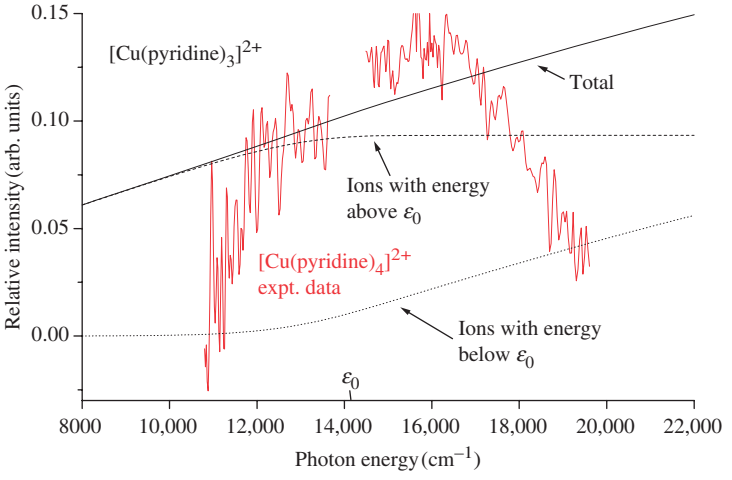

Figure 7. [Colour online] Photofragment yields plotted as a function of photon energy. The calculated data are for $[Cu(pyridine)_3]^{2+}$ and have been determined from the kinetic equations presented in the text, and where the contributions from above and below ε_0 correspond to the regions identified in Figure 5. The experimental data were recorded for $[Cu(pyridine)_4]^{2+}$ [37].

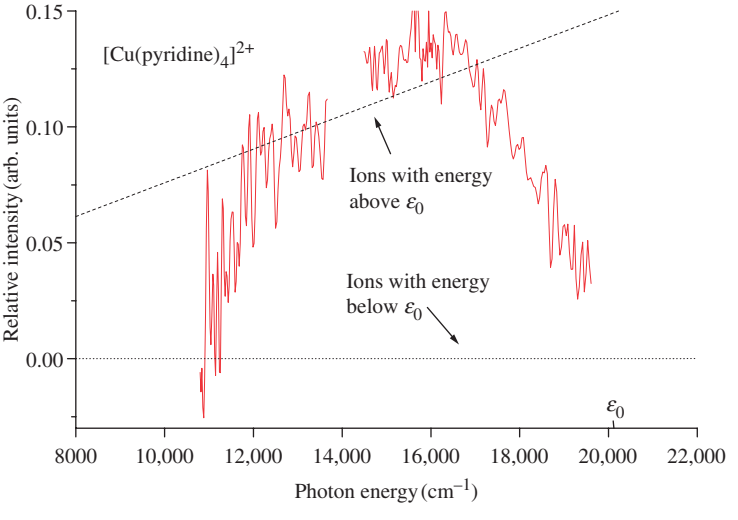

Figure 8. [Colour online] Similar to Figure 7, but the calculations and the experimental data are for $[Cu(pyridine)_4]^{2+}$.

From the results presented thus far it is obvious that there are going to be circumstances under which 'cold' ions will not photodissociate, and that the only opportunity for recording spectra at visible wavelengths is when ions retain a high level of vibrational excitation from the preparation process (electron impact ionisation).

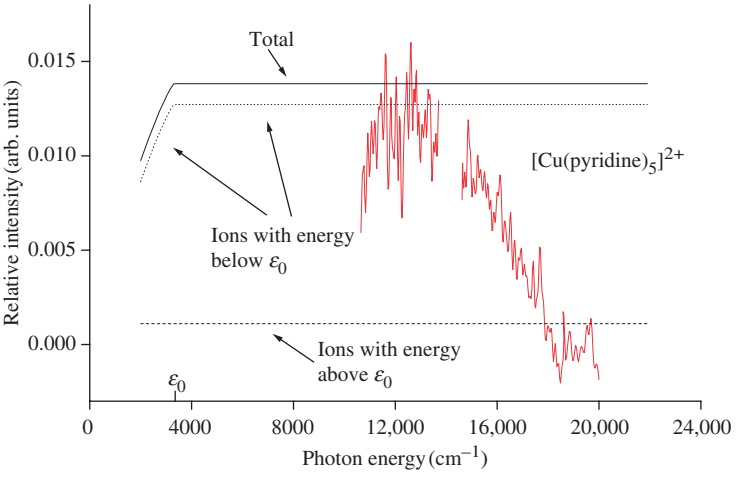

Figure 9. [Colour online] Similar to Figure 7, but the calculations and the experimental data are for $[Cu(pyridine)_5]^{2+}$.

However, the degree of thermal broadening associated with these ions will, in turn, reduce the spectral resolution that can be achieved. An alternative strategy might be to tag the complexes with a rare gas atom, along similar lines to those currently used to record IR spectra from cold ions. There are two obvious problems with this approach. First, for doubly charged complexes, the binding energies of rare gas atoms can be quite high (~1 eV) [47], which means that there could still be a problem where residual internal energy influences spectra recorded towards the red end of the electromagnetic spectrum. However, a more significant problem will be a structural one, a central tenet of LF spectroscopy is the influence different ligand (field) geometric configurations have on spectral transitions [32]. If, for example, an argon atom is added to $[Cu(pyridine)_4]^{2+}$, a complex that is probably square-planar in its most stable form [37], will be forced towards a square-pyramidal geometry, with obvious consequences for the spectroscopy.

For complexes with high binding energies, the situation does not improve significantly if photons of a higher energy are used. The $[Cu(pyridine)_N]^{2+}$ series has also been studied at UV wavelengths (266 nm) where known charge transfer transitions have been observed [48]. Figure 10 illustrates what excitation at UV wavelengths means in terms of overcoming ligand binding energies, and it can be seen that all fragmentation pathways are accessible (apart from $N \leq 2$). For $[Cu(pyridine)_4]^{2+}$, which is the complex with the highest binding energy, Figure 11 shows that the calculated total ion yield now includes contributions from the two separate energy regions (Equations 3 and 4) identified in Figure 5. Even at these much higher photon energies, a significant fraction of the ion yield still comes from 'hot' ions, and it is only at energies $>35{,}000\,cm^{-1}$ that ions from below ε_0 begin to contribute to the signal. Even then, these latter ions still contain a high internal energy prior to photoexcitation. What makes a significant contribution to this pattern of behaviour is a kinetic shift imposed by the time constraint that photoexcited ions have to fragment within their flight time ($\sim 10^{-4}$ s) through the excitation region. To illustrate this point, this last calculation on $[Cu(pyridine)_4]^{2+}$ has been repeated, but with a timescale

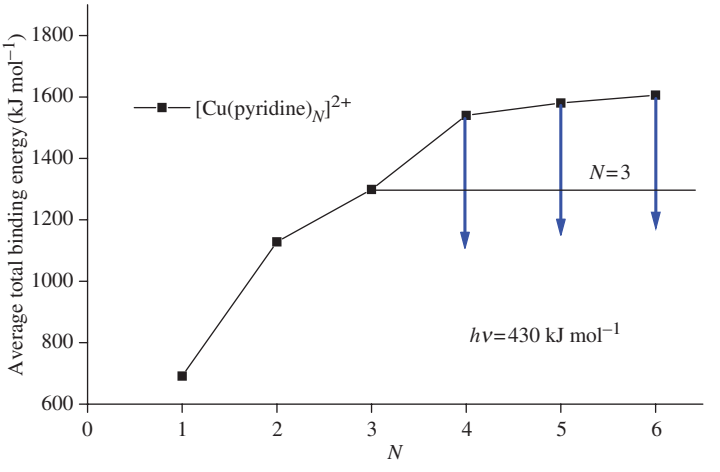

Figure 10. [Colour online] Similar to Figure 6, but the photon energy is 430 kJ mol^{-1} (35,900 cm^{-1}).

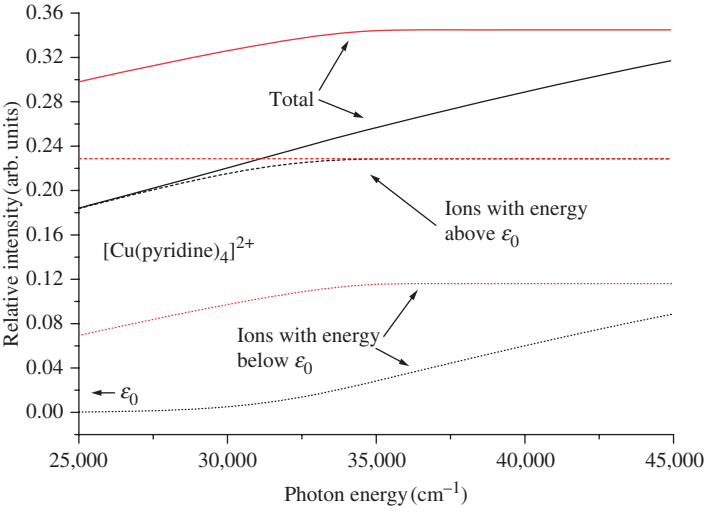

Figure 11. [Colour online] Calculated photofragment yields from [Cu(pyridine)$_4$]$^{2+}$ excited at UV wavelengths. The lines in black denote where the experimental time scale is ~10^{-4} s, and the lines in red denote an ion trap experiment where the duration (storage time) is 1 s.

that is more appropriate for an experiment performed in an ion trap. In Equations (3) and (4), t_4 has been increased to 1 s, which is probably an upper limit on the storage time required for an experiment of this nature. These results are also shown in Figure 11, where it can be seen that the consequences of a kinetic shift are evident. The contribution from ions with internal energy > ε_0 rapidly reaches saturation, but for those ions with energy below ε_0, the extra time afforded by their residence in the trap increases the opportunity to fragment. Overall, the total photofragment signal at ~25,000 cm^{-1} is predicted to be twice

that of a similar experiment in a sector mass spectrometer. Obviously, other factors, such as radiative decay, will increase in significance for experiments undertaken in a trap, and so at best, these calculations can only be viewed as semi-quantitative in terms of estimating photofragment yields.

One final factor that has implications for all of the calculations discussed here is the development of techniques whereby ions can be cooled prior to photoexcitation. Most such experiments are based on an ion trap where ions are held in the presence of a cold helium buffer gas, and temperatures as low as 10 K have been reported for large molecular systems [40]. Similar experiments involving metal dications complexes are not so advanced and to date, the lowest temperature achieved is in the region of 100–150 K. Looking at Figures 5–11, it is obvious that cooling will have a significant influence on exactly what type of experiment can be performed. If the internal energies of the various ions drop by a substantial amount, then all of those fragmentation processes that rely on ions with an energy $>\varepsilon_0$ will not be observed and no spectra will be recorded. For obvious reasons, increasing the photon energy will improve matters, and as Figure 11 shows, storing ions for as long as possible following photoexcitation will minimise effects imposed by a kinetic shift. What may prove impossible without some form of $(1+1)$ two-photon experiment is the ability to record LF spectra at visible wavelengths for a range of different-sized complexes. For example, Figures 8 and 9 show that recording photofragmentation spectra from cold ions would be possible at ~600 nm for $[Cu(pyridine)_{5,6}]^{2+}$ but not for $[Cu(pyridine)_4]^{2+}$.

There is one further caveat to this analysis and that is the possibility that photofragmentation does not follow a unimolecular or RRKM style pathway. Such an exception might be where excitation is to a strongly antibonding orbital of the complex where the excited ion sits on a repulsive surface and fragments before there is any opportunity for relaxation or intersystems crossing. An obvious example of this would be photoexcitation followed by charge transfer. Figure 3 shows good evidence of where this type of fragmentation (reaction 2 using linearly polarised laser radiation) has taken place on a timescale that is short compared to the rotational period of the ion ($\sim 10^{-11}$ s), and is many orders of magnitude shorter than the timescales that are responsible for the behaviour predicted in Figure 8. However, as noted earlier, signal recovery then becomes an issue for sector mass spectrometers, but not so for ion traps, where charge transfer products are routinely recorded.

4. Theory section

Currently, the most commonly used single-reference theory for modelling excited states of medium-sized and large molecules is TDDFT [31], attested by the fact that two Special Issues on TDDFT appeared in 2009 [49] and [50]. Casida's linear response formulation of TDDFT for calculating excitation spectra made implementation into existing quantum chemistry software codes possible [51] and since then TDDFT has developed into a well-established method for treating electronic excited states [52]. Although an exact TDDFT exchange-correlation (XC) functional would give all spectroscopically allowed transitions, including those with many-electron character, virtually all implementations in popular codes invoke the adiabatic approximation, which assumes that the XC-potential reacts instantaneously and without memory of any temporal change in the charge density.

It is also well established that only one-electron excitations are available from adiabatic TDDFT [51].

There has been much discussion of the well-documented limitations of TDDFT, in particular when treating Rydberg excitations and long-range charge-transfer (CT) excitation. It has been shown that the ionisation continuum in the linear-response TDDFT excitation spectrum begins at minus the energy of the highest occupied molecular orbital ($-\varepsilon_{\mathrm{HOMO}}$) and due to the necessary use of inexact XC-functionals the TDDFT ionisation threshold is too low. This leads to an early onset of the ionisation continuum, resulting in bound Rydberg states falling into an artificially low ionisation continuum [53]. The error in Rydberg excitations can be improved through the application of an asymptotic correction (e.g. [54–57]), or by using an optimised effective potential (OEP) to generate 'exact exchange' sometimes called the EXX method (e.g. [58–61]; see also recent work using an orbital-dependent non-adiabatic exchange kernel [62]). For the dication metal–ligand complexes considered here, the electronic excitation energies are all considerably lower than $-\varepsilon_{\mathrm{HOMO}}$ (the ionisation threshold) and thus adiabatic TDDFT is valid for their excitation energies [53]. However, the use of an asymptotically correct (ac) XC potential, such as SAOP (statistical average of different orbital model potentials with exact asymptotic behaviour for the highest occupied KS orbital) [63], stabilises the orbital energies, and whilst this is important for an accurate description of Rydberg excited states [64,65], it can also provide a consistent description of bound state excitations [43,66].

Particularly pertinent to this work is the well-documented underestimation of long-range CT excitations [67–70]. However, it appears to date that LMCT and MLCT transitions in multiply charged metal–ligand complexes, do not appear to suffer from what can be a substantial (1–2 eV) underestimation of the CT transition energy [43,71,72]. Tozer *et al*. [73,74] have provided a possible explanation of this behaviour *via* their lambda diagnostic test which states that if the spatial overlap between the occupied and virtual orbitals involved in a transition is small then the error in the CT excitation will be large. Although one cannot be sure that a large overlap implies a small error [75], it provides a possible explanation for the reasonable agreement between calculated TDDFT and experimental spectra of multiply charged metal–ligand complexes [43]. By construction, states with high oscillator strengths such as those considered for comparison with experiment have high lambda values, and the dominant UV/Vis excitations in multiply charged metal–ligand complexes involve metal–ligand molecular orbitals with electron density spread across several atoms, therefore facilitating good spatial overlap between the occupied and virtual orbitals, thus it provides an explanation for the, sometimes, excellent agreement with experiment (see below). In fact, it has been suggested that 'problem' CT excitations are perhaps better referred to as 'density transfer excitations' since many CT excitations in chemistry, involve little or no density transfer and therefore show no particular problem when described with TDDFT [52].

One final particularly important consideration for work associated with metal dication complexes is double- or higher-excitations, which cannot be modelled by adiabatic TDDFT. It has been stated that explicit many electron excitations are needed for a proper description of excitations of molecules with open-shell ground states [76,77]. In fact, in 1996, Maurice and Head-Gordon [78] proposed that the meaning of excitation levels as used for closed-shell ground states should be redefined for open-shell radicals.

They showed, with reference to the doublet state, that there exists a spin-adapted configuration that is neither a single nor double substitution but is a mixture of the two with the correct multiplicity to describe the doublet excited states. Maurice and Head-Gordon [78] included this 'extended' class of excitation in their implementation of the CIS method (XCIS). In a subsequent article, Hirata and Head-Gordon [79] questioned whether the use of existing functionals with the adiabatic approximation can properly account for excitations that have significant two-electron character. Both Hirata and Head-Gordon [79] by comparison with their XCIS method (which provided a useful quantitative measure of the percentage of double excitation character in the excited states of the small radicals considered), and Tozer *et al*. [80] by comparison with CASPT2 calculations on tetrazine, have shown that whilst doubly excited states do not appear in a TDDFT spectrum (which in principle contains only the single excitation manifold), the mainly singly excited states with a large contribution from doubly excited configurations do appear and their excitation energy are no less accurate than the pure singly excited states, that is whilst linear response TDDFT misses the pure double excitations it can work reasonably well when there is significant double excitation character. More recently, Ipatov *et al*. [81] have shown that some excited states of open-shell molecules will have unphysically large amounts of spin contamination that can result in physically incorrect or missing states. (Spin contamination has also been discussed in the context of ground state DFT [82] where the authors argue that a KS determinant for an open-shell system which is *not* spin-contaminated is wrong! This is because spin-unrestricted Hartree–Fock wavefunctions are described as spin-contaminated as they are not pure eigenfunctions of the total spin operator $\widehat{S}^2$, but since the determinant of KS orbitals is not the correct wavefunction for the system it is necessarily spin-contaminated, that is since the single determinant of KS orbitals refers to a non-interacting system rather than the real system, spin-contamination is not a problem.) Ipatov *et al*. [81] state that for molecules with open-shell ground states, 'one can at best trust only those excited states which preserve the expectation value of $\widehat{S}^2$, and even then it is possible that some peaks [excitations] will be missing'. To help identify nonphysical solutions so that they can either be removed or improved, Ipatov *et al*. [81] present equations for calculating the spin contamination of TDDFT states. The most serious spin contamination routinely encountered in TDDFT appears to be of a type that results from an absence of the double and higher excitations needed to correctly describe spin–permuted configurations. These excitations can be identified by assigning spin symmetries using the formula they present and hence removed or corrected. Furthermore, Ipatov *et al*. [81] find that the physically meaningful excitation energies in the systems they considered are almost exclusively simple excitations involving the singly occupied molecular orbital (SOMO).

A solution to these problems, i.e. the lack of multi-electron excitations in TDDFT due to the adiabatic approximation, is to allow the coupling matrix to be frequency dependent. Frequency-dependent XC-kernels are now beginning to be investigated [76, 83–85,77]. In fact, Casida ([52], p.15) in 2009 states that 'Going beyond the TDDFT adiabatic approximation to include frequency dependence in the XC-kernel seems urgent' and that 'fundamental studies are certainly welcome as relatively little is known about the frequency dependence of the exact $f_{xc}(\omega)$'. Certainly, if theory is to provide an interpretation of the new state-resolved spectra emerging from recent experiments on open-shell complexes, then 'urgent' is absolutely right.

4.1. *Ground state calculations*

Electronic spectra calculated using TDDFT (vertical excitations) are very sensitive to the ground state geometry of a complex. Therefore, the inclusion or omission of relativistic effects (e.g. through the zeroth-order regular approximation, ZORA [86,66]) in transition metal–ligand complexes (second row and beyond) can not only influence transition energies, but can also alter the overall shape of an absorption profile through changes to the relative oscillator strengths of transitions. When considering the electronic ground state of a gas phase complex, it is important to take account of all possible structural isomers. The nature of either of the two techniques currently used to generate multiply charged metal–ligand complexes in the gas phase, pick-up and electrospray, is such that ions will be formed with a certain amount of internal excitation. In terms of Figure 5, the level of excitation could be up to ε_0, the lowest dissociation energy, which means that any geometric isomers with potential energies at or below this value could be accessible, and in the absence of collisions or radiative decay there will be no mechanism for quenching these down to the lowest energy structure.

Evidence of how geometric isomers might influence observations made on the metal dication complexes are to be seen in the recent literature. The first two examples come from studies of Sn^{2+} and Cu^{2+}-hydrates. Theory and experiment shows that the formation of charge-enhanced hydrogen bonds makes it possible for solvent molecules to begin participating in the formation of a second solvation shell before the first is complete [87]. Calculations (ccsd(t)/6-31 + G(d,p)//MP2/6-31 + G(d,p) with a Stuttgart/Dresden effective core potential (SDD) on the metal dication) have shown that for the $[Sn(H_2O)_4]^{2+}$ complex two geometric structures are prevalent [88]. These are a 'butterfly structure' and a '3 + 1' structure, which are shown in Figure 12 and differ in energy by just 8 kJ mol^{-1} ($\sim$3 kT at 298 K). In a compilation of extended X-ray absorption fine structure (EXAFS) data, Ohtaki and Radnai [89] suggested that Sn^{2+} is a peculiar ion in that it has a hydration structure that is less symmetrical than other $d^{10}s^2$ ions, as two separate bond distances have been observed in the six-coordinated hydration structure, one 2.33–2.34 Å and the other 2.38–2.90 Å. The calculations showed that both structures (the butterfly and the 3 + 1), each have two separate bond distances, and the bond lengths associated with the butterfly structure in particular, at 2.34 and 2.47 Å, are in excellent agreement with the range covered by the experimental data. It has been suggested that these alternative structural isomers facilitates early proton transfer, and provides an explanation for the anomalous acidities of Sn(II) and Pb(II) [88]. In the case of Cu^{2+}, evidence of similar behaviour comes from calculations by Bérces *et al.* [90]. An experimental study of $[Cu(H_2O)_N]^{2+}$ and $[Cu(NH_3)_N]^{2+}$ complexes showed that those where $N = 8$ are the most intense [10], and to explain this Bérces *et al.* [90] proposed structures that consist of a square-planar arrangement of water or ammonia molecules to which a further four molecules are attached *via* double-acceptor hydrogen bonds. However, a more recent experimental study by O'Brien and Williams [91], where multiphoton IR excitation has been used to record vibrational spectra, shows the above structure for $[Cu(H_2O)_8]^{2+}$ to be just one of several hydrogen bonded permutations to be contained within the ion signal observed for the complex. The literature contains many examples of geometric isomers having been observed for hydrated complexes of singly charged metal ions [87].

It would appear that these hydrogen bonded networks could have a strong influence on the development of gas phase $[ML_N]^{z+}$ structures; although, when considering geometries

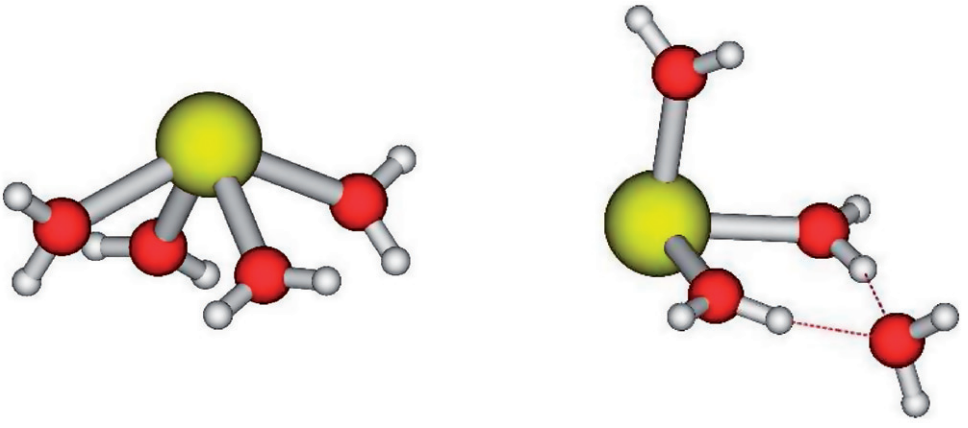

Figure 12. [Colour online] Examples of the isomeric structures calculated at the MP2/6 − 31 + *G*(d,p) level of theory for $[Sn(H_2O)_4]^{2+}$ [88].

that use hydrogen bonding to go beyond the first coordination shell, DFT is not usually the best approach [92]. However, recent developments by Grimme *et al*. [93,94] to include an empirical correction to account for dispersion may be an appropriate way forward. It will be of interest to determine how the Grimme [93] GGA-D functionals compare with meta-hybrid GGA's such as the newly developed M06 density functional [95] and with DF-LMP2 (density-fitted local MP2), [96] methods in the treatment of hydrogen bonding in solvent shells surrounding metal dications and as a function of computational cost.

A third example of isomerisation is based on calculations undertaken to account for visible spectra recorded for the complexes $[Cu(pyridine)_4]^{2+}$ and $[Ag(pyridine)_4]^{2+}$ [37,43]. Both of these ions should have square-planar D_{4h} structures, but calculations showed that a D_{2h} structure (rotation of two of the pyridine rings) and a tetrahedral–like D_{2d} structure were all within approximately 40 kJ mol^{-1} of the ground state for $[Cu(pyridine)_4]^{2+}$ and within 60 kJ mol^{-1} for the case of $[Ag(pyridine)_4]^{2+}$. Given that the ligand binding energy in a complex, such as $[Ag(pyridine)_4]^{2+}$, is ~200 kJ mol^{-1}, the interpretation of any photodissociation spectra would need to take all of these structures into account.

The accuracy of ground state binding energies and geometries using standard DFT is well established. For example, bond lengths are usually within a few pm of the experimental values, and Zhao and Truhlar [97] have shown that the maximum mean unsigned error (MUE) for the bond lengths of metal containing diatomics calculated with a range of functionals (meta-GGA, hybrid and GGA) is 0.013 Å. Likewise, the MUE for a database of metal–ligand bond energies (using hybrid-meta-GGA, meta-GGA, hybrid and GGA functionals) is 8.3 [98] and 8.1 kcal mol^{-1} when including the M06 functional and a slightly different set of functionals [95].

The newly developed M06-suite of density functionals (including the hybrid-meta-GGA (M06) and the local meta-GGA (M06-L) functionals) were produced specifically for treating main group and transition metal chemistry, and they have been shown to perform exceptionally well for organometallic and transition metal energetics [95]. These functionals would appear to be good candidates for future DFT work on transition

metal dications. Recent calculations on $Cu^+(pyridine)_N$ at the M06-L/6–311 ++ G(d,p) level of theory (including BSSE and zero point energy) have shown that the binding energy of Cu^+-pyridine is within 2 kJ mol^{-1} of that determined experimentally [99] with an error that increases to just 8 kJ mol^{-1} for the fourth ligand binding energy (i.e. the energy of the reaction $[Cu(pyridine)_4]^+ \rightarrow [Cu(pyridine)_3]^+ +$ pyridine), and for the four-coordinate $[Cu(pyridine)_4]^+$ complex the error in the average binding energy (i.e. $[Cu(pyridine)_4]^+ \rightarrow Cu^+ + 4$ pyridine) is just 17 kJ mol^{-1} [100].

4.2. *Excited state calculations*

In a typical spectroscopic study of metal–ion complexes, it is assumed that the absorption of a single photon leads to photodissociation such that a photofragment spectrum reflects an absorption spectrum. The only circumstance under which that assumption may breakdown is when the binding energy of a ligand becomes larger than the energy of a photon. In general, it would appear that, for experiments performed at UV wavelengths, this assumption holds true; however, at visible wavelengths it has been shown above that the observation of photofragments can depend on the internal energy content of the ions, the radiation wavelength and the time scale over which observations are made.

The shape and width of a band in a photofragment spectrum results from vibronic transitions where an excitation of one or more vibrational modes occur simultaneously with the electronic transition. Nevertheless, it is usual to interpret spectra by comparing calculated vertical excitation energies with the maxima in the absorption spectrum. Dierksen and Grimme [101] have investigated the vibronic structure of electronic absorption spectra of large organic molecules using TDDFT and calculating the frequencies of the optimised excited state within the harmonic approximation. They found that the vibronic structure of strongly dipole allowed transitions (calculated within the Franck–Condon approximation) were in very good agreement with the experiment, and weakly dipole-allowed and dipole-forbidden transitions (calculated within the Franck–Condon–Herzberg–Teller and Herzberg–Teller approximations, respectively) were slightly more problematic, but that the TDDFT approach to calculated vibronic structure seems to be superior to other more sophisticated methods. Of particular relevance to the future work described in this review is their conclusion that the vibronic structure of strongly dipole-allowed transitions can routinely be calculated on the basis of TDDFT methods. Furthermore, they noted that the difference between vertical and 0–0 excitation energies diminishes as the size of the molecule increases, and thus it seems possible to use calculated vertical excitation energies, especially for larger compounds or when trends in a series of systems are considered. Thus, in the work described here, we have generally compared vertical excitation energies calculated using adiabatic TDDFT with the maximum in the band of an electronic transition.

It would appear that DFT as implemented in the Amsterdam density functional (ADF) software [102], performs particularly well for open shell transition metal complexes, easily finding stable states with close lying spin-multiplicities (e.g. high spin and low spin). Work on $[Cu(pyridine)_4]^{2+}$ and $[Ag(pyridine)_4]^{2+}$ complexes using the DFT–ΔSCF method demonstrated that the method was sufficient to explain spectral features of Cu(II)– and Ag(II)–pyridine photodissociation spectra [37]. DFT–ΔSCF can be used to explore the lowest lying energy state of any spatial irreducible representation (or indeed

spin multiplicity) as that state represents the 'ground state' in that particular symmetry (or that particular spin state), but it is not suitable for second (or higher) excited states of a particular symmetry, and oscillator strengths are not readily available with this method.

With the subsequent implementation of open-shell TDDFT in commonly used quantum chemistry packages such as ADF [103–106] this has now become the principal method for exploring the electronically excited states of multiply charged metal–ligand complexes. Excitation energies and oscillator strengths calculated using TDDFT involve a self-consistent field (SCF) step and a post SCF step. The SCF step yields KS orbitals and orbital energies (and for this there is the usual choice of XC functionals in addition to the specifically designed asymptotically correct XC potentials such as SAOP [63]) and the post SCF step produces excitation energies and oscillator strengths and uses the adiabatic local density approximation (ALDA) [107]. However, the best choice of functional (in terms of agreement with experimental spectra) appears to depend on the metal complex, and in many cases, an asymptotically correct functional is the most appropriate regardless of the fact that the excitation energies are considerably below the ionisation threshold, $-\varepsilon_{HOMO}$ [53]. Thus, as with the use of ground state DFT a functional evaluation (used for the SCF step) is recommended. It is also possible to apply the Tamm–Damcoff approximation (TDDFT/TDA) [108] to obtain the excitation energies; this simplifies the algebra and associated algorithms and leads to a reduction in the computational cost without significant deviations from the TDDFT excitation energies [64]. A TZ2P basis set (with or without inclusion of relativistic effects through ZORA [86]) is usually sufficient for consistent valence excited state data for both open-shell (doublet) and closed-shell metal ligand complexes and TDDFT gives excitation energies for transitions involving valence states with surprisingly good accuracy including LMCT as discussed above.

In a recent study of the visible spectra of Ag^{2+} complexes, [43] TDDFT was used to successfully explain the following experimental observations: (i) the $[Ag(acetone)_4]^{2+}$ spectrum peaked at $\sim$18,500 cm^{-1}; (ii) this absorption feature was red—shifted with respect to that of $[Ag(pyridine)_4]^{2+}$ which peaked at $\sim$21,500 cm^{-1}; (iii) no spectrum could be recorded for $[Ag(acetonitrile)_4]^{2+}$ and (iv) none of the spectra recorded for larger complexes ($n > 4$) showed any evidence of Jahn–Teller distortion on the part of the d^9 metal dication. In all cases, the incremental binding energies were lower than the onset energy at which photofragmentation was observed. The binding energy of a fourth ligand to the $[Ag(ligand)_3]^{2+}$ complex were calculated to be: 162 kJ mol^{-1} (13,500 cm^{-1}) for pyridine; 137 kJ mol^{-1} (11,500 cm^{-1}) for acetone and 180 kJ mol^{-1} (15,000 cm^{-1}) for acetonitrile. The absence of an experimental spectrum for the $[Ag(acetonitrile)_4]^{2+}$ complex at visible wavelengths was explained satisfactorily by TDDFT, which showed that the first dipole-allowed transition requires a photon energy in excess of 40,000 cm^{-1}. Interestingly, this experimental/theoretical observation also matches what is seen for condensed phase complexes involving $[Ag(acetonitrile)_4]^{2+}$, which are known to be white solids.

Figure 13 shows examples of recorded and calculated LDA(ALDA)/TZP(ZORA) spectra for $[Ag(acetone)_N]^{2+}$ complexes for $N = 4$–6. In any study of this kind, it is of interest to understand how the development of solvent structure influences electronic structure and, as a consequence, the evolution of spectra. The experimental spectra show a slight blue-shift ($\sim$1500 cm^{-1}) of the absorption maxima for $N = 5$ and 6 relative to that of $N = 4$, which is reproduced in the calculations (the strongest bands of the

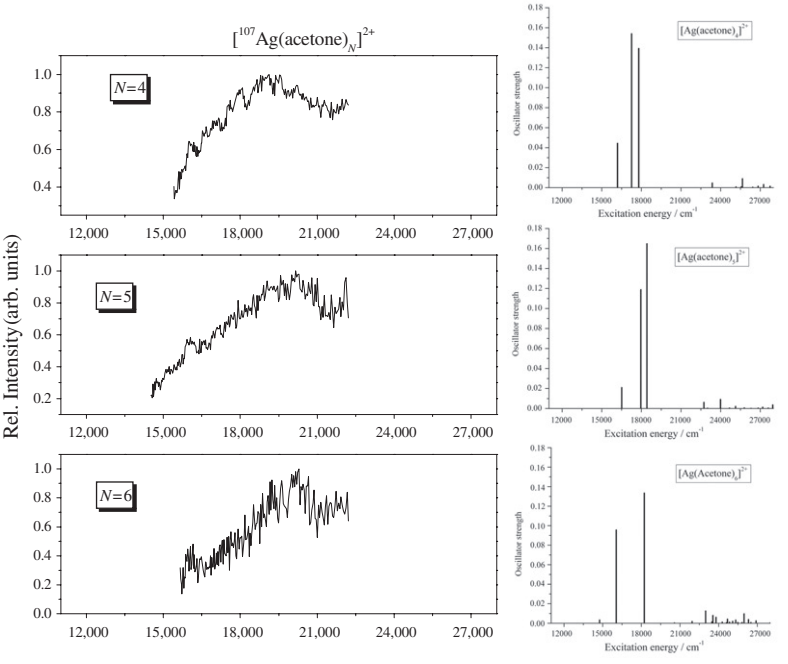

Figure 13. Experimental and calculated (TDDFT) spectra for $[Ag(acetone)_N]^{2+}$, $N = 4$–6. Adapted with permission from [43]. Copyright 2007, American Institute of Physics, but using LDA(ALDA)/TZP(AE)ZORA TDDFT data rather than SAOP(ALDA)/TZP(AE)ZORA as presented in Ref [43].

$[Ag(acetone)_{5,6}]^{2+}$ complexes have blue-shifts relative to that of $N = 4$ of 1161 and 971 cm^{-1}, respectively); this effect in the experimental data could be as a consequence of the internal energy content of the ions, where the lower binding energies of the $N = 5$ and 6 ions mean that most photodissociation takes place from comparatively cold ions with energies below ε_0 (Figure 9). Given that the calculations (as expected) show the $N = 5$ and 6 complexes to be severely Jahn–Teller distorted, it is perhaps surprising that these weakly-bound ligands did not have more of an influence on profiles recorded for their photodissociation spectra. However, the absence of an obvious Jahn–Teller effect was common to all of the ligands studied (N– and O–coordinating) [43]; the reason being that the ligands subject to distortion did not contribute electron density to the molecular orbitals involved in the excitation spectra. What is clear from Figure 13 is that there is a very good match between the TDDFT electronic excitation energies and oscillator strengths with the observed absorption maxima (agreement to within 2000 $cm^{-1} = 0.25$ eV). However, it is also clear that the 2–3 calculated excitations could cover a range of wavelengths under the broad absorption band, and thus it is not clear exactly how many electronic excitations contribute to the recorded spectra.

In the recent article by Ipatov *et al.* [81], it was noted that the spectra of doublet systems, such as Cu^{2+} and Ag^{2+}, are most likely to be effected by spin contamination. Nevertheless, given the broadness of the experimental features and their close overlap with the calculated excitations, it is possible to give a semi-quantitative interpretation of the spectra. The appropriate transition is dominated by the movement of a beta electron from

a doubly occupied orbital to the $d_{x^2-y^2}$ SOMO, i.e. it is a LMCT transition, which compares well both with the experimental observation of a ligand cation as a major photofragment and with the estimated extinction coefficient of 500 L mol^{-1} [37], the latter value being close in magnitude to that considered appropriate for a Laporte-allowed charge transfer transition involving an aromatic molecule [32]. Molecular orbital analysis reveals that both the 'ligand based' orbital and 'metal-based' orbital involve electron density on several ligands. Furthermore, given that the dominant transition involves the movement of a beta-electron into the SOMO rather than the movement of an alpha-electron from the SOMO into an unoccupied orbital, the simple assumption that LMCT transitions bear some relation to the ionisation energy of the ligand concerned does not hold [43]. This statement is supported by the observation that spectra for the acetone complexes are red-shifted relative to those of the pyridine complexes, despite the fact that the ordering of the ionisation energies is pyridine < acetone.

Since ions are required to have electronic transitions that are capable of excitation at the wavelengths used, it is assumed that the reaction products of photoexcitation can be related to the nature of the excitation. For example, LMCT transitions could result in ligand cation as opposed to neutral loss, but these assertions are yet to be confirmed *via* quantitative studies. Fortunately, due to the pioneering work of Van Caillie and Amos [109], and extended by Furche and Ahlrichs [110], excited state (TDDFT) gradients and frequencies have recently become readily available in popular quantum chemistry software packages such as Gaussian [111], and this information will make it possible to optimise excited states. Thus, future work should involve exploration of excited states and routes to photodissociation (previously this latter step has often been performed in small molecules by stepping along a defined reaction coordinate, see, e.g. [112] or [64]). Exploring excited state surfaces and photodissociation pathways will provide definitive answers regarding current assumptions on the origins of the observed reaction products. This is potentially very rewarding because, in addition to being able to assign state-resolved photofragmentation spectra with reasonable accuracy in many cases, there is also the opportunity to understand the physics of photofragmentation processes. Possible electronic excitation/photofragmentation pathways may include: (i) excitation to a purely repulsive excited state surface (resulting in rapid cation ligand loss); (ii) excitation to a bound state with an asymptote below the ground state asymptote or (iii) excitation to a bound excited state that undergoes curve crossing to a repulsive CT curve, which means that vertical excitations can lead to spectra that are not directly representative of the observed fragmentation products. Thus, there is a significant amount of new information about the behaviour of the ground and excited states of multiply charged metal–ligand complexes to be derived from these calculations. This new insight will provide the potential to control and modify the behaviour of these same cations in future gas phase experiments and ultimately the condensed phase.

Improvements in experimental technique and principally the development of methods for cooling ions have lead to the observation of UV spectra with significantly better resolution than was possible in earlier experiments (Figure 13). This is certainly the case for $[Zn(pyridine)_4]^{2+}$, where it has been possible to resolve features due to individual electronic transitions [113]. Calculations on the structure and electronic excitation energies of the $[Zn(pyridine)_4]^{2+}$ complex were performed using TDDFT (LDA(ALDA)/TZ2P) as implemented in the ADF program [102,103,114,115]. To help in the interpretation

of excitation spectra, calculations were also performed on the pyridine molecule at the same level of theory. The calculations showed there were no dipole-allowed transitions below 37,000 cm^{-1}, and in fact the theory successfully guided the experiment to locate a very prominent spectral feature at 41,100 cm^{-1}. However, it was unclear whether the observed features were the result of multiple electronic excitations (Figure 14a) or of a single electronic excitation, which was coupled to an excited vibrational mode (Figure 14b), thus both possibilities were explored. Vibrations in the ground state were coupled with the first electronically allowed excitation (a ^{1}E: $\pi^* \leftarrow \pi$ transition), and the assignment of electronic transitions was based on TDDFT calculations. (As mentioned above, previous TDDFT calculations on $[Ag(acetone)_4]^{2+}$ and $[Ag(pyridine)_4]^{2+}$, showed those systems to have relatively few electronic excitations within a broad absorption band recorded at visible wavelengths.) Both of the above possibilities provided a reasonable interpretation of the experimental data. However, the first calculated transition to have a significant oscillator strength ($\sim$0.005) at 38020 cm^{-1}, came within 250 cm^{-1} (0.03 eV) of an experimental feature, and for at least eight of the calculated transitions there were peaks in the experimental spectrum that are within 550 cm^{-1} (0.07 eV) of the predicted excitation energies. Therefore, it was concluded that excitation of such a complex is essentially adiabatic and that the spectrum is largely electronic; however, a vibrational progression cannot not be dismissed completely.

Further analysis showed the transitions observed for the $[Zn(pyridine)_4]^{2+}$ complex to fall into three categories according to oscillator strength, f: (i) $f \geq 0.01$; these closely matched the experimental features purely in terms of dominance, and were in excellent quantitative agreement with the experiment; (ii) $0.01 > f \geq 0.003$; these excitations were assigned purely according to position and relative (rather than absolute) magnitude, but again there was good agreement and (iii) $f < 0.003$; these transitions are not observed experimentally. Thus, these data provided a good indication of oscillator strengths (or more precisely, orders of relative magnitude) to an accuracy required for predicting the spectra of multiple charge metal–ligand complexes.

Due to the closed-shell nature of the $[Zn(pyridine)_4]^{2+}$ complex, TDDFT performed exceptionally well and it was possible to not only assign the experimental spectra but to also guide the experiment to the locations of undetected features outside the initial spectra search range [113]. The agreement between the experiment and calculations, in terms of excitation energy and dominance (oscillator strength), was exceptional and of an accuracy greater than that of vastly more sophisticated wavefunction-based methods. However, the quality of the experimental spectra reported sets demanding new tests for theory, and to truly understand the fine structure (and be confident that a single-reference method is adequate), methods capable of optimising excited state geometries (and including MR character) appears to be an important next step.

Most recently, adiabatic TDDFT has been used with considerably less success to calculate the vertical electronic excitation of the open-shell, high-spin (sextet) $[Mn(pyridine)_4]^{2+}$ complex, for which an experimental spectrum of a similar quality to that recorded for the closed-shell $[Zn(pyridine)_4]^{2+}$ complex has been produced [116]. The excited states of molecules with high-spin ground states can be divided into four types (see Figure 1 of Ref. [117]) [78]. Types 1 and 2 refer to excitations that involve the SOMO; type 1 involves alpha spin electron promotion from a SOMO to a valence orbital; type 2 involves beta spin electron promotion from a doubly occupied orbital to a singly

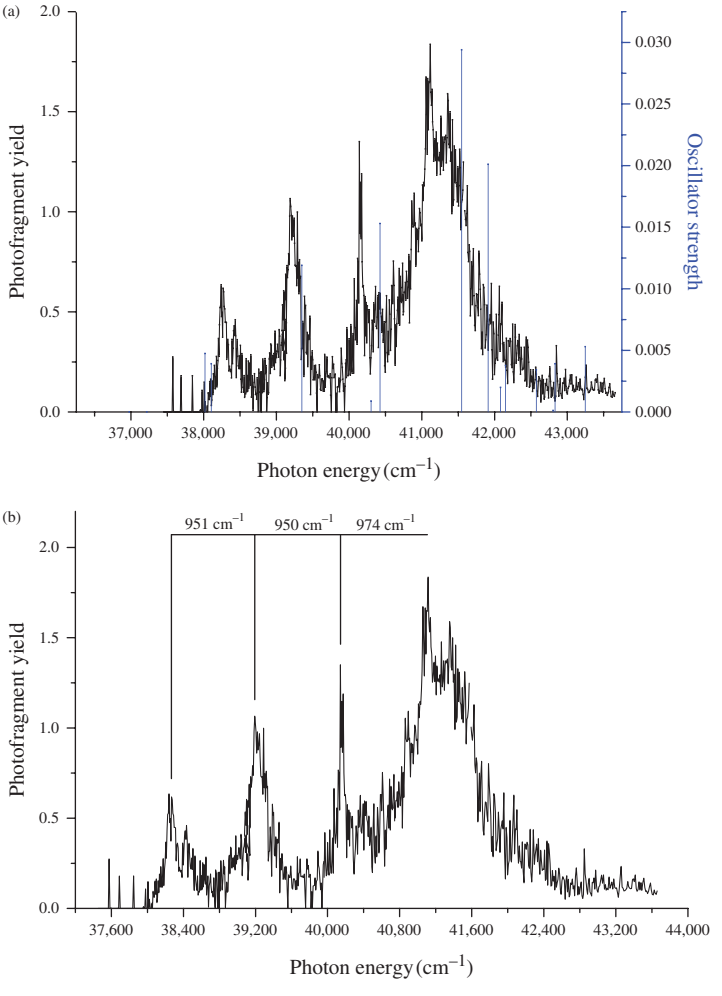

Figure 14. [Colour online] Comparison between the experimental UV spectrum recorded for $[Zn(pyridine)_4]^{2+}$ and two possible interpretations: (a) multiple electronic transitions: stick spectra calculated using TDDFT (LDA(ALDA)/TZ2P(AE)) and (b) vibrational structure embedded within a single electronic transition.

occupied orbital. These types of excitation in open-shell molecules have a single excitation character and are well described by adiabatic TDDFT. Also Ipatov *et al.* [81] have shown that excitations involving the SOMO should present no particular problem regarding spin-contamination. In type 3 and type 4 excitations, the SOMO is nominally a spectator. Type 3 excitations are described either by a single electron promotion from a doubly occupied orbital to a virtual orbital or alternatively by promotion of an alpha spin electron from a SOMO and the simultaneous promotion of a beta spin electron into the singly occupied orbital vacated by the first excitation. Type 4 excitations are described by the simultaneous promotion of two electrons: one from a singly occupied orbital to a virtual

orbital and another electron from a doubly occupied orbital to a singly occupied orbital, but different from that involved in the first excitation. However, this analysis has been based on a restricted formulism [117], whereas the calculations in computational codes such as ADF employ unrestricted different orbitals for different spin (DODS) procedure, and so it is not possible to uniquely define the singly occupied orbitals. Additionally, the beta unoccupied orbitals may not match the half-occupied alpha orbitals in character (or even symmetry) [78]. Furthermore, Ipatov *et al*. [81] have shown that for the case where the SOMO is nominally a spectator (i.e. types 3 and 4), the problem of three (or more) coupled spins arises, which in the case of a doublet ground state, leads to a quartet and two doublet excited states, and the doublet states can mix.

Given the sextet ground state of $[Mn(pyridine)_4]^{2+}$ and thus the need for the excited state method to describe double- and higher-excitation characters of this open-shell complex, the results of single-electron excitations as described by adiabatic TDDFT calculations were not considered to be sufficiently reliable or accurate to identify the discrete electronic transitions that appear in the spectrum and make a quantitative assignment of the experimental data. As mentioned previously, TDDFT is in principle capable of providing a full description of the system with an exact frequency-dependent XC functional; however, in the absence of the latter, TDDFT is restricted to strictly one-electron excitations. Furthermore, there is no way of telling if an excitation from a TDDFT calculation has double excitation character without performing a XCIS or MR calculation. Complexes, such as $[Mn(pyridine)_4]^{2+}$ highlight some of the problems that arise when using the standard adiabatic implementations of TDDFT to describe open-shell complexes where multi-excitation character can dominate the excited states [116]. However, there have been recent theoretical developments that attempt to go beyond the standard adiabatic approximation and consider the frequency dependence required for a non-adiabatic TDDFT approach (as discussed in the Theory section), which may then begin to address many of the issues highlighted.

5. Conclusion

The development of new methods for generating and studying multiply charged metal–ligands complexes in the gas phase has created opportunities for studying metal ions in their more common charge states. The pick-up technique [3,15] has been shown to yield complexes that contain a very diverse range of ligands, whilst electrospray [8,16] offers the advantage of generating complexes of a more biological nature. In this review, we have focused on the measurement and interpretation of electronic spectra and included in this category is the possibility of recording LF spectra in the gas phase. Although, at first sight, the weak absorption cross-sections that accompany *d–d* spectral transitions would appear to present a substantial obstacle to reliable signal detection, calculations presented here would suggest that ligand binding energy and the need to overcome that energy barrier to detect a photofragment signal, presents a more significant, and indeed, a more general obstacle to recording state-resolved electronic spectra. Unless the binding energy is very low ($< h\nu$), ions have to rely on residual internal energy to assist dissociation, which in turn, means a loss of spectral resolution. The use of rare gas tagging does not present an obvious solution, because even closed-shell atoms, such as argon, can have quite high binding energies to metal dications [47]. Furthermore, an important aspect of

LF spectroscopy is structure, and the perturbations introduced by the presence of a rare gas atom could influence ligand configuration. Overall, the prospect of achieving vibrational state resolution in gas phase LF spectroscopy is a challenge for which there is, as yet, no obvious solution. Where significant progress has been made is in the recording of UV spectra [113,116] and this has been achieved because the energy of a typical photon ($\sim$5 eV) is now significantly larger than a typical ligand binding energy. A slight disadvantage of experiments at UV wavelengths is that many ligand–ligand electronic transitions are observed; however, when it comes to studying closed-shell metal dications, e.g. Zn^{2+} [113] the benefits are that the influence of the charge can be tracked through the perturbation it has on ligand orbitals.

As the resolution of these experiments improves the challenge for theory in terms of understanding the fine structure increases. It is clear both adiabatic and non-adiabatic processes must be considered to ensure that all of the physics presented in the spectra is captured. For this, it will be necessary to optimise excited states to determine the extent to which the excited state is distorted, analyse their vibrational structure and determine routes to dissociation. A major future goal will be to determine the applicability of commonly used single-reference methods (adiabatic TDDFT, new developments/implementations of non-adiabatic TDDFT) by comparing with more sophisticated MR wavefunction-based methods and to access the effect of spin-orbit coupling on vertical excitations (initially using TDDFT [86]) and its role in inter-system crossings (using e.g. MRCI). The benefits of this work are two-fold: (i) it will account for the photodissociation products, provide mechanisms and allow calculation of the life times of excited states; if the latter are purely repulsive (and/or transition states) this would suggest experimental opportunities to probe LF excited states of cold ions and obtain spectra with the resolution recently produced in the UV [113, 116]; (ii) the systematic comparison of vertical excitation data/ground state geometries with optimised excited state geometries, frequencies and routes to photodissocation will provide important data on the ability of the vertical excitation methods to capture the essence of the processes involved in photodissociation experiments and hence assign the resulting spectra; this can be used to establish a guide so that larger systems (where system size makes high-level MR calculations unfeasible) can be tackled with confidence.

From recent observations on the electronic spectra of metal dication complexes [113,116] it is apparent that, for excited states, it is not sufficient to validate the theoretical method by just comparing the ground state structural and energetic data of the complex with experiment. Some of the most recently recorded electronic spectra are yielding energy level differences to an accuracy of 500 cm^{-1}, and as a result these are beginning to establish new and more demanding benchmarks for theoretical methods.

Acknowledgements

The authors are indebted to Dr Ljiljana Puškar for her perseverance and expertise in making many of the measurements outlined both here and in other published work on this topic, and to Dr Guohua Wu for his work on development of the ion trap experiment. The authors would also like to thank EPSRC for financial support and the EPSRC National Service for Computational Chemistry Software for computer time: URL http://www.nsccs.ac.uk.

References

[1] P. Kebarle, Annu. Rev. Phys. Chem. **74**, 1466 (1977).
[2] R. G. Keesee and A. W. Castleman Jr, J. Phys. Chem. Ref. Data **15**, 1011 (1986).
[3] A. J. Stace, J. Phys. Chem. A **106**, 7993 (2002).
[4] F. A. Cotton and G. Wilkinson, *Advanced Inorganic Chemistry* (Wiley, London, 1988).
[5] L. Puškar, X. Chen, and A. J. Stace (unpublished).
[6] H. Cox, R. R. Wright, N. R. Walker, and A. J. Stace, J. Am. Chem. Soc. **125**, 233 (2003).
[7] M. Kohler and J. A. Leary, J. Am. Soc. Mass Spectrom. **8**, 1124 (1997).
[8] A. T. Blades, P. Jayaweera, M. G. Ikonomou, and P. Kebarle, Int. J. Mass Spectrom. Ion Processes **102**, 251 (1990).
[9] C. J. Thompson, J. Husband, F. Aguirre, and R. B. Metz, J. Phys. Chem. A **102**, 7779 (1998).
[10] A. J. Stace, N. R. Walker, and S. Firth, J. Am. Chem. Soc. **119**, 10239 (1997).
[11] N. R. Walker, S. Firth, and A. J. Stace, Chem. Phys. Lett. **292**, 125 (1998).
[12] R. R. Wright, N. R. Walker, S. Firth, and A. J. Stace, J. Phys. Chem. A **105**, 54 (2001).
[13] X. Yang, X. B. Wang, and L. S. Wang, J. Phys. Chem. A **106**, 7607 (2002).
[14] X. B. Wang, A. P. Sergeeva, J. Yang, X. P. Xing, A. L. Boldyrev, and L. S. Wang, J. Phys. Chem. A **113**, 5567 (2009).
[15] L. Puskar, K. Tomlins, B. Duncombe, H. Cox, and A. J. Stace, J. Am. Chem. Soc. **127**, 7559 (2005).
[16] A. T. Blades, P. Jayaweera, M. G. Ikonomou, and P. Kebarle, J. Chem. Phys. **92**, 5900 (1990).
[17] M. A. Duncan, Annu. Rev. Phys. Chem. **48**, 69 (1997).
[18] T. D. Vaden and J. M. Lisy, J. Phys. Chem. A **109**, 3880 (2005).
[19] N. R. Walker, R. S. Walter, and M. A. Duncan, New J. Chem. **29**, 1495 (2005).
[20] E. D. Pillai, T. D. Jaeger, and M. A. Duncan, J. Phys. Chem. A **109**, 3521 (2005).
[21] (a) A. Klamt and G. Schüürmann, J. Chem. Soc. Perkin Trans **2**, 799 (1993); (b) A. Klamt, J. Phys. Chem. **99**, 2224 (1995).
[22] S. Miertus and J. Tomasi, Chem. Phys. **65**, 239 (1982).
[23] A. Vlcek Jr and S. Záliš, Coord. Chem. Rev. **251**, 258 (2007).
[24] J. Roithová and D. Schröder, Coord. Chem. Rev. **253**, 666 (2009).
[25] W. Koch and M. C. Holthausen, *A Chemist's Guide to Density Functional Theory* (Wiley-VCH, Weinheim, 2001).
[26] C. J Cramer and D. G. Truhlar, Phys. Chem. Chem. Phys. **11**, 10757 (2009).
[27] J. P. Perdew and K. Schmidt, in *Density Functional Theory and its Applications to Materials*, edited by V. Van Doren, C. van Alsenoy, and P. Geerlings (AIP press, New York, 2001).
[28] J. P. Perdew, A. Ruzsinszky, J. Tao, V. N. Staroverov, G. E. Scuseria, and G. I. Csonka, J. Chem. Phys. **123**, 062201 (2005).
[29] S. F. Sousa, P. A. Fernandes, and M. J. Ramos, J. Phys. Chem. A **111**, 10439 (2007).
[30] L. Serrano-Andres and M. Merchan, J. Mol. Struct. Theochem **729**, 99 (2005).
[31] A. Dreuw and M. Head-Gordon, Chem. Rev. **105**, 4009 (2005).
[32] A. B. P. Lever, *Inorganic Electronic Spectroscopy* (Elsevier, Amsterdam, 1984).
[33] T. G. Spence, B. T. Trotter, T. D. Burns, and L. A. Posey, J. Phys. Chem. A **102**, 6101 (1998).
[34] C. J. Thompson, K. P. Faherty, K. L. Stringer, and R. B. Metz, Phys. Chem. Chem. Phys. **7**, 814 (2005).
[35] R. B. Metz, Int. J. Mass Spectrom. **235**, 131 (2004).
[36] L. Puškar and A. J. Stace, J. Chem. Phys. **114**, 6499 (2001).
[37] L. Puškar, H. Cox, A. Goren, G. D. C. Aitken, and A. J. Stace, Faraday Disuss. **124**, 259 (2003).
[38] R. G. Cooks, J. H. Beynon, R. M. Caprioli, and G. R. Lester, *Metastable Ions* (Elsevier, Amsterdam, 1973).
[39] G. Wu, D. Chapman, and A. J. Stace, Int. J. Mass Spectrom. **262**, 211 (2007).

[40] D. Gerlich, in *Advances in Chemical Physics*, Vol. LXXXII, edited by C. Ng and M. Baer (J. Wiley, New York, 1992, p. 1).
[41] K. P. Faherty, C. J. Thompson, F. Aguirre, J. Michne, and R. B. Metz, J. Phys. Chem. A **105**, 10054 (2001).
[42] M.T. Bowers, editor, *Gas Phase Ion Chemistry, Ions and Light,* 3 Vols. (Academic Press, New York, 1984).
[43] J. Guan, L. Puškar, R. O. Esplugas, H. Cox, and A. J. Stace, J. Chem. Phys. **127**, 064311 (2007).
[44] W. Forst, *Theory of Unimolecular Reactions* (Academic Press, New York, 1973).
[45] A. J. Stace and C. Moore, J. Am. Chem. Soc. **105**, 1814 (1983).
[46] Adapted from data given in ref. [37].
[47] N. R. Walker, R. R. Wright, P. E. Barran, H. Cox, and A. J. Stace, J. Chem. Phys. **114**, 5562 (2001).
[48] L. Puškar, P. E. Barran, R. R. Wright, D. A. Kirkwood, and A. J. Stace, J. Chem. Phys. **112**, 7751 (2000).
[49] M. A. L. Marques and A. Rubio, Phys. Chem. Chem. Phys. **11**(22), 4421–4688 (special issue) (2009).
[50] M. E. Casida, H. Chermette, and D. Jacquemin, J. Mol. Struct. Theochem **914**, 1–138 (special issue) (2009).
[51] M. E. Casida, Time-dependent density functional response theory for molecules, in *Recent Advances in Density Functional Methods*, Part I, edited by D.P. Chong (World Scientific, Singapore, 1995, p. 155).
[52] M. E. Casida, J. Mol. Struct. Theochem **914**, 3 (2009).
[53] M. E. Casida, C. Jamorski, K. C. Casida, and D. R. Salahub, J. Chem. Phys. **108**, 4439 (1998).
[54] M. E. Casida, K. C. Casida, and D. R. Salahub, Int. J. Quant. Chem. **70**, 933 (1998).
[55] D. J. Tozer and N. C. Handy, J. Chem. Phys. **109**, 10180 (1998).
[56] M. E. Casida and D. R. Salahub, J. Chem. Phys. **113**, 8918 (2000).
[57] S. Hirata, C. G. Zhan, E. Apra, T. L. Windlys, and D. A. Dixon, J. Phys. Chem. **107**, 10154 (2003).
[58] J. D. Talman and W. F. Shadwick, Phys. Rev. A **14**, 36 (1976).
[59] A. Görling, Phys. Rev. Lett. **83**, 5462 (1999).
[60] S. Ivanov, S. Hirata, and R. J. Bartlett, Phys. Rev. Lett. **83**, 5455 (1999).
[61] A. Heßelmann and A. Görling, Chem. Phys. Lett. **455**, 110 (2008).
[62] A. N. Ipatov, J. Expt. Th. Phys. **100** (2), 199 (2010).
[63] O. V. Gritsenko, P. R. T. Schipper, and E. J. Baerends, Chem. Phys. Letts. **302**, 199 (1999).
[64] J. Guan, F. Wang, T. Ziegler, and H. Cox, J. Chem. Phys. **125**, 044314 (2006).
[65] M. Grüning, O. V. Gritsenko, S. J. A. van Gisbergen, and E. J. Baerends, J. Chem. Phys. **116**, 9591 (2002).
[66] F. Wang, T. Ziegler, E. van Lenthe, S. van Gisbergen, and E. J. Baerends, J. Chem. Phys. **122**, 204103 (2005).
[67] A. Dreuw, J. L. Weisman, and M. Head-Gordon, J. Chem. Phys. **119**, 2943 (2003).
[68] D. J. Tozer, J. Chem. Phys. **119**, 12697 (2003).
[69] A. Dreuw and M. Head-Gordon, J. Am. Chem. Soc. **126**, 4007 (2004).
[70] O. Gritsenko and E. J. Baerends, J. Chem. Phys. **121**, 655 (2004).
[71] C. Norris, D. Phil. thesis, University of Sussex, 2009.
[72] R. O. Esplugas, D. Phil. thesis, University of Sussex, 2009.
[73] M. J. G. Peach, P. Benfield, T. Helgaker, and D. J. Tozer, J. Chem. Phys. **128**, 044118 (2008).
[74] M. J. G. Peach and D. J. Tozer, J. Mol. Struct. Theochem **914**, 110 (2009).
[75] M. J. G. Peach, C. R. Le Sueur, K. Ruud, M. Guillaume, and D. J. Tozer, Phys. Chem. Chem. Phys. **11**, 4465 (2009).
[76] P. Romaniello, D. Sangalli, J. A. Berger, F. Sottile, L. G. Molinari, L. Reining, and G. Onida, J. Chem. Phys. **130**, 044108 (2009).

[77] M. E. Casida, J. Chem. Phys. **122**, 054111 (2005).
[78] D. Maurice and M. Head-Gordon, J. Phys. Chem. **100**, 6131 (1996).
[79] S. Hirata and M. Head-Gordon, Chem. Phys. Lett. **302**, 375 (1999).
[80] D. J. Tozer, R. D. Amos, N. C. Handy, B. O. Roos, and L. Serrano-Andrés, Mol. Phys. **97**, 859 (1999).
[81] A. Ipatov, F. Cordova, L. J. Doriol, and M. E. Casida, J. Mol. Struct. Theochem **914**, 60 (2009).
[82] J. A. Pople, P. M. W. Gill, and N. C. Handy, Int. J. Quantum Chem. **56**, 303 (1995).
[83] N. T. Maitra, F. Zhang, R. J. Cave, and K. Burke, J. Chem. Phys. **120**, 5932 (2004).
[84] R. J. Cave, F. Zhang, N. T. Maitra, and K. Burke, Chem. Phys. Lett. **389**, 39 (2004).
[85] O. V. Gritsenko and E. J. Baerends, Phys. Chem. Chem. Phys. **11**, 4640 (2009).
[86] E. van Lenthe, A. E. Ehlers, and E. J. Baerends, J. Chem. Phys. **110**, 8943 (1999).
[87] A. J. Stace, Phys. Chem. Chem. Phys. **3**, 1935 (2001).
[88] H. Cox and A. J. Stace, J. Am. Chem. Soc. **126**, 3939 (2004).
[89] H. Ohtaki and R. Radnai, Chem. Rev. **93**, 1157 (1993).
[90] A. Bérces, T. Nukada, P. Margl, and T. Ziegler, J. Phys. Chem. A **103**, 9693 (1999).
[91] J. T. O'Brien and E. R. Williams, J. Phys. Chem. **112**, 5893 (2008).
[92] F. P. Rotzinger, J. Phys. Chem. B **109**, 1510 (2005).
[93] S. Grimme, J. Comput. Chem. **25**, 1463 (2004).
[94] S. Grimme, J. Antony, T. Schwabe, and C. Mück-Lichtenfeld, Org. Biomol. Chem. **5**, 741 (2007).
[95] Y. Zhao and D. G. Truhlar, Theor. Chem. Accounts **120**, 215 (2008); Table 19, p. 235.
[96] H. J. Werner, F. R. Manby, and P. J. Knowles, J. Chem. Phys. **118**, 8149 (2003).
[97] Y. Zhao and D. G Truhlar, J. Chem. Phys. **125**, 194101 (2006); Table XII, pp. 194101–14.
[98] See Reference 97, Table VII, pp. 194101–10.
[99] N. S. Rannulu and M. T. Rodgers, J. Phys. Chem. A **111**, 3465 (2007).
[100] C. Norris, G. Wu, J. Guan, S. Hessey, H. Cox, and A. J. Stace (in preparation).
[101] M. Dierksen and S. Grimme, J. Chem. Phys. **120**, 3544 (2004).
[102] ADF, SCM, Theoretical Chemistry, Vrije Universiteit, Amsterdam, The Netherlands, <http://www.scm.com>.
[103] S. J. A. van Gisbergen, J. G. Snijders, and E. J. Baerends, Comput. Phys. Commun. **118**, 119 (1999).
[104] F. Wang and T. Ziegler, Mol. Phys. **102**, 2585 (2004).
[105] F. Wang and T. Ziegler, J. Chem. Phys. **121**, 12191 (2004).
[106] F. Wang and T. Ziegler, J. Chem. Phys. **122**, 074109 (2005).
[107] E. K. U. Gross and W. Kohn, Adv. Quant. Chem. **21**, 255, (1990).
[108] S. Hirata and M. Head-Gordon, Chem. Phys. Lett. **314**, 291, (1999).
[109] C. Van Caillie and R. D. Amos, Chem. Phys. Lett. **308**, 249 (1999); **317**, 159 (2000).
[110] F. Furche and R. Ahlrichs, J. Chem. Phys. **117**, 7433 (2002).
[111] M. J. Frisch, G. W. Trucks, H. B. Schlegel, G. E. Scuseria, M. A. Robb, J. R. Cheeseman, G. Scalmani, V. Barone, B. Mennucci, G. A. Petersson, H. Nakatsuji, M. Caricato, X. Li, H. P. Hratchian, A. F. Izmaylov, J. Bloino, G. Zheng, J. L. Sonnenberg, M. Hada, M. Ehara, K. Toyota, R. Fukuda, J. Hasegawa, M. Ishida, T. Nakajima, Y. Honda, O. Kitao, H. Nakai, T. Vreven, J. A. Montgomery, Jr, J. E. Peralta, F. Ogliaro, M. Bearpark, J. J. Heyd, E. Brothers, K. N. Kudin, V. N. Staroverov, R. Kobayashi, J. Normand, K. Raghavachari, A. Rendell, J. C. Burant, S. S. Iyengar, J. Tomasi, M. Cossi, N. Rega, J. M. Millam, M. Klene, J. E. Knox, J. B. Cross, V. Bakken, C. Adamo, J. Jaramillo, R. Gomperts, R. E. Stratmann, O. Yazyev, A. J. Austin, R. Cammi, C. Pomelli, J. W. Ochterski, R. L. Martin, K. Morokuma, V. G. Zakrzewski, G. A. Voth, P. Salvador, J. J. Dannenberg, S. Dapprich, A. D. Daniels, O. Farkas, J. B. Foresman, J. V. Ortiz, J. Cioslowski, and D. J. Fox, *Gaussian 09, Revision A.02*, Gaussian, Inc., Wallingford, CT, 2009.

[112] M. Citir and R. B. Metz, J. Chem. Phys. **128**, 024307 (2008).
[113] G. Wu, C. Norris, H. Stewart, H. Cox, and A. J. Stace, Chem. Comm. **35**, 4153–4155 (2008).
[114] G. te Velde, F. M. Bickelhaupt, S. J. A. van Gisbergen, C. Fonseca Guerra, E. J. Baerends, J. G. Snijders, and T. Ziegler, J. Comput. Chem. **22**, 931 (2001).
[115] A. Rosa, E. J. Baerends, S. J. A. van Gisbergen, E. van Lenthe, J. A. Groeneveld, and J. G. Snijders, J. Am. Chem. Soc. **121**, 10356 (1999).
[116] G. Wu, H. Stewart, F. D. Lemon, H. Cox, and A. J. Stace, Mol. Phys. **108**, 1199 (2010).
[117] Z. Rinkevicius, I. Tunell, P. Salek, O. Vahtras, and H. Ågren, J. Chem. Phys. **119**, 34 (2003).